Available online at www.sciencedirect.com

ScienceDirect

Current Opinion in
Colloid & Interface Science

Modeling drop deformations and rheology of dilute to dense emulsions

Rodrigo B. Reboucas, Nadia N. Nikolova and Vivek Sharma

We highlight the current state-of-the-art in modeling emulsion rheology, ranging from dilute to jammed dense systems. We focus on analytical and numerical methods developed for calculating, computing, and tracking drop deformation in response to viscometric flows and deriving constitutive models for flowing emulsions. We identify material properties and dimensionless parameters, collate and catalog the small deformation theories and resulting expressions for viscometric quantities, and take stock of challenges for capturing connections between drop deformation, morphology, and rheology of emulsions. We highlight the substantial progress in providing quantitative descriptions of the rheological response using analytical theories, scaling, and computational fluid dynamics. We illustrate how macroscopic rheological properties emerge from microscopic features including the deformation and dynamics of noninteracting or interacting drops, and molecular aspects that control the interfacial properties.

Addresses
University of Illinois Chicago, 929 W Taylor Street, Chicago, 60608 IL, USA

Corresponding authors: Reboucas, Rodrigo B. (rodrigobentoo@gmail.com); Sharma, Vivek (viveks@uic.edu)

Current Opinion in Colloid & Interface Science 2025, **77:**101904

This review comes from a themed issue on **Rheology**

Edited by: **Ruth Cardinaels** and **Yujun Feng**

For a complete overview see the Issue and the Editorial

https://doi.org/10.1016/j.cocis.2025.101904

Keywords
drop deformation, emulsion rheology, food science, yield stress, colloidal dispersions, fizzics, interfacial science.

Introduction

Emulsions are dispersions of droplets in a continuous suspending liquid phase [1–4]. Examples of emulsions include food materials such as milk, creams, salad dressings, chocolate, and mayonnaise, and cosmetics marketed as lotions and creams. Pharmaceutical formulations like certain eye drops, skin care lotions, and oral emulsions are designed such that the oil phase serves as a carrier for certain hydrophobic bioactives. Dispersion of crude oil drops in water during petroleum extraction or in oceans after oil spills produces oil-water petroleum emulsions. Blends of immiscible polymer solutions or melts that contain droplets dispersed in a suspending liquid are also emulsions. The immiscibility implies that the free energy of the mixing is higher than the phase-separated systems formed by drops in a matrix phase [4]. The formulation of emulsions with flow properties suitable for processing, applications, and sensory perception involves quests that belong to the realm of rheology, i.e. the science of deformation and flow of simple and complex fluids (or soft matter) [3–6]. Emulsion rheology is characterized by measuring the response to applied stress, strain, or strain rate, typically using specialized equipment called rheometers that are designed to create viscometric flows or well-defined flow fields to assess flow behavior [3–5]. The deformability of drops, the possibility of flow within them, and their coalescence or breakup contribute to emulsion rheology [1–4] can be quite distinct from the rheology of complex fluids containing dispersed particles, micelles, or macromolecules [4–16]. Furthermore, the stability and flow behavior of emulsions depend on the composition, structure, and mechanical properties of the interface between the dispersed and continuous phases [17–21]. In this contribution, we highlight how size, shape, concentration, interactions, and interfacial properties of dispersed drops influence droplet concentration-dependent variation in the rheological response of emulsions.

Processing operations such as pumping, dispensing, pouring, spreading, and even emulsion stability or shelf life are influenced by shear viscosity η, which characterizes resistance to shear flows associated with velocity gradients perpendicular to the flow direction [4,5]. Such shear flows commonly arise near solid-liquid interfaces, including pressure-driven flows through channels, and drag flows around immersed objects or near moving substrates. Most published emulsion rheology studies primarily describe the magnitude and measurement of shear viscosity, η, with a focus on stress or shear rate dependent variation [4,8,10,20,22–24]. However, streamwise velocity gradients associated with extensional or elongational flows commonly arise in converging channels, porous media, and free surface flows, involving the formation of liquid necks that undergo capillarity-driven pinching [4,5]. Studies of extensional rheology of emulsions are less common due to longstanding experimental and modeling challenges [25–28]. Extensional rheology responses profoundly influence the processing, applications, and consumer use and perception of emulsions, described in heuristic terms such as sprayability, jettability, stringiness, and ropiness [25–28].

Spherical drops deform into ellipsoidal shapes in response to weak velocity gradients [11–15,20] and can undergo large deformations in response to strong flows, forming slender bodies, and even undergoing capillarity-driven pinching leading to breakup [29–32]. Emulsification or emulsion formation, liquid blending, and emulsion rheology are three important problems that involve drop deformations in response to flow fields [20,32–36]. Analytical approaches capture minor or small deformations from spherical shape, but numerical approaches are necessary to model large deformations and pinching, breakup, or coalescence of drops, especially, for emulsions containing the dispersed drop phase in higher volume fractions.

Emulsion drops deformed by velocity gradients display elasticity due to restoring stresses set by interfacial tension. After the flow stops, drops can recover their unperturbed spherical shape, as it is the minimum energy configuration for a fixed drop volume [12]. The characteristic timescale for recovering this interfacial energy-favored state is called relaxation time [12] though the terms shape or surface tension relaxation time are also used in the emulsion rheology literature [4,9,20]. The shape relaxation time appears as viscocapillary time in interfacial fluid mechanics, including the studies of pinching, coalescence, and spreading of drops [37,38] as it captures the interplay of viscous and interfacial stresses. A somewhat analogous elastic response is displayed in dilute polymer solutions by polymer chains perturbed by flow, and here, a relaxation time is defined as the characteristic time over which the unperturbed, entropically favored coiled state is recovered after the cessation of the flow [4,39]. In both dilute emulsions and polymer solutions, this elastic recovery of the unperturbed drop shape or coil configuration is at the heart of viscoelastic behavior, captured as modulus in stress relaxation and oscillatory shear measurements, or manifested in steady shear torsional rheometry as a normal force or elastic instability due to nonzero normal stress differences [4,5].

In nondilute emulsions and particle suspensions, pairwise and higher-order interactions and the local arrangement of discrete drops or particles constitute the microstructure that influences the flow behavior [4–6,8]. In-situ visualization or monitoring of the evolution of microstructure in flow fields by optical or spectroscopic methods shows that the rearrangement, deformation and orientation of drops together determine the rheological response, including rate variation of shear viscosity and normal stress differences and amplitude and frequency-dependent moduli measured using oscillatory shear [20,29,30,32,40]. In the jammed dense emulsion, the shear flow behavior is also influenced by deformation and flows in interconnected liquid films, leading to a yield stress that must be exceeded before flow can be observed, and typically, shear viscosity measured post-yielding exhibits a deformation rate- or stress-dependent nonlinear response [41–44]. Due to the enhanced nonlinearity and complexity of the problems, few studies explore the response of the nondilute emulsions in extensional flows and confined flows [45]. Far fewer theoretical and simulation studies account for the influence of non-Newtonian response (rate-dependent shear and extensional viscosity, transient, and nonlinear viscoelasticity) of the suspending or dispersed liquid or of the decorated, populated interface [45].

In this brief review, we highlight theoretical and numerical advances in modeling flows of dilute to dense jammed emulsions. The review is divided into six sections. Emulsion microhydrodynamics: the governing equations and scaling: includes motivation, scope, brief history, definitions, transport equations, and dimensional analysis. Dilute emulsions: small deformation theory and consitutive models presents the small deformation theory and constitutive models for dilute emulsions. Incorporating three cases: clean drops, surfactact-covered drops and drops with slip at an interface. Nondilute emulsions: constitutive models and numerical methods describes the changes in emulsion rheology due to an increase in the number density of drops, includes a discussion of small deformation theory and alternative constitutive models, and provides a survey of numerical methods developed for nondilute emulsions, highlighting their strengths and weaknesses. The next section – jammed dense emulsions with polygonal drops in a network of films – presents a short survey of various models outlined for jammed dense emulsions that display properties that are foamlike. Challenges, opportunities, and prognosis section closes this overview by highlighting a few open problems and opportunities for theorists and computational scientists. We have included a primer on the small deformation theory in Appendices A and B, retracing steps taken by Frankel and Acrivos [15] from the shape distortion tensor to the constitutive equation for dilute emulsions that can describe both transient and steady state non-Newtonian and viscoelastic response of emulsions.

Classifying emulsions and mapping concentration-dependent rheology

Classifying emulsions Emulsions are classified using many criteria, ranging from the choice of dispersed and suspending liquid, interface composition, application (food, pharmaceutical, personal care and cosmetics, petroleum), and drop size and volume fraction range

[1–3,46,47]. Emulsions are often described on the basis of the choice of dispersed and suspending phase, oil-water or water-oil emulsions that can be obtained by mechanical mixing, phase separation, microfluidics, vapor condensation, or biologically, as in milk. Here, oil can refer to vegetable oils, crude oil (or derived oil), silicone oils, polymerizable monomers (in latex), or even organic liquids, while the water phase can be made with an aqueous solution or water-based mixed solvent. Both milk and mayo are examples of oil-water emulsions, containing water as the suspending or continuous liquid. Unlike such emulsions, water-in-water emulsions spontaneously appear as complex coacervate forms between two oppositely charged polyelectrolytes and phase separates forming emulsions that are unstable and have a short shelf-life [48], though recent studies describe attempts to enhance stability against coalescence [49].

Typical household emulsions, such as milk, mayonnaise, cosmetic lotions and creams, salad dressings, and fabric softeners appear milky due to scattering by drops with sizes greater than the wavelength of visible light (drop sizes, a >1 micron). These are examples of macroemulsions, and being thermodynamically unstable, have a finite shelf life that can be enhanced by reducing drop sizes and size dispersity, diminishing density difference, increasing the suspending fluid viscosity or manipulating drop–drop interactions [1–3,7]. Like macroemulsions, nanoemulsions (sometimes called miniemulsions) are also thermodynamically unstable, but smaller drop sizes (a = 50–500 nm) and tighter control over size dispersity lead to prolonged kinetic stability [1,50–52]. In contrast, microemulsions that have relatively small drop sizes (a = 10–100 nm) are thermodynamically stable and appear transparent. Classification based on interface composition: small molecule surfactants (including soaps or detergents), flexible or globular proteins, lipids, particles, polymers, or their complexes emphasizes the critical role played by adsorbed species in influencing the flow properties and stability of emulsions [1,3,20].

Concentration-dependent regimes: dilute to jammed dense Constitutive equations that model the flow properties of emulsions consider the influence of number density, interactions, and deformation of drops [1,4,8,10,22,23,47]. The exhibited rheological behavior is considered a linear response if the measured flow properties (stress, viscosity, or modulus) do not depend on the impelling quantities (stress, strain, or strain rate). Dilute emulsions exhibit viscosity or resistance to flow that is comparable to suspending fluid, as can be observed for animal milks, which are examples of emulsions with a relatively low ϕ of dispersed drops. In the dilute regime, the macroscopic properties that capture the linear viscoelastic response, including η_0, increase linearly with ϕ. The deformation and hydrodynamics of each drop in dilute emulsion can be considered independently, by neglecting the influence of hydrodynamic and thermodynamic interactions. In semidilute emulsions, pairwise interactions make relative viscosity exhibit a nonlinear increase with ϕ. In concentrated emulsions, drops are so closely packed that drop mobility and deformation become highly restricted by caging or surrounding drops. The shear viscosity exhibits a stronger non-Newtonian response for the nondilute emulsions, and the elastic effects become progressively stronger with an increase in ϕ. The semidilute to highly concentrated emulsions contain a progressively higher ϕ (or number density of drops) and influence of associative and repulsive interdrop interactions and microstructure become manifest and measurable [1,8,16,53].

Figure 1 illustrates that four concentration regimes, dilute, semidilute, concentrated, and highly concentrated emulsions, can be identified by examining the variation in relative viscosity, η_r on increasing droplet volume fraction, ϕ. Here $\eta_r = \eta/\mu$ representing the emulsion's zero shear viscosity scaled with suspending fluid viscosity, μ. Viscosity increases with ϕ substantially in the highly concentrated regime, qualitatively emulating the behavior of rigid particle suspensions, where viscosity diverges close to maximum volume fraction [7,54,55]. Due to the deformability of drops, droplet volume fraction can be increased further, leading to the jammed dense emulsion regime. As the volume fraction of drops lies beyond the maximum packing fraction for spherical or ellipsoidal particles, jammed dense emulsions contain polygonal-shaped drops separated by interconnected liquid films with a foam-like microstructure. Mayonnaise, an egg-based emulsion of vegetable oil droplets suspended in an aqueous medium [28], is an example of jammed dense emulsion containing closely packed, polygonal drops, with a volume fraction of the drop phase between $\sim 65\% - 80\%$. Such dense emulsions display yield stress, τ_Y, and elastic modulus, G, that increases with volume fraction [1,4,8,23].The variation in yield stress and modulus scaled by capillary pressure is illustrated in the Figure 1 for jammed dense emulsions. Though it is well-established that increasing drop volume fraction leads to a transition from suspension-like to foam-like behavior, as shown schematically, for emulsion drops, and for deformable particles, the transition region depends on many factors, including size and shape, size dispersity, interactions, and mechanisms underlying the deformability of the dispersed phase [1,7,8,56,57].

Highlights from ninety years of analytical models for emulsion rheology The review encompasses and primarily highlights models that rely on small deformation theory, a perturbation calculation for weak deviations about a spherical shape that are apt for dilute emulsions, and provide insights into the rheology of nondilute

Figure 1

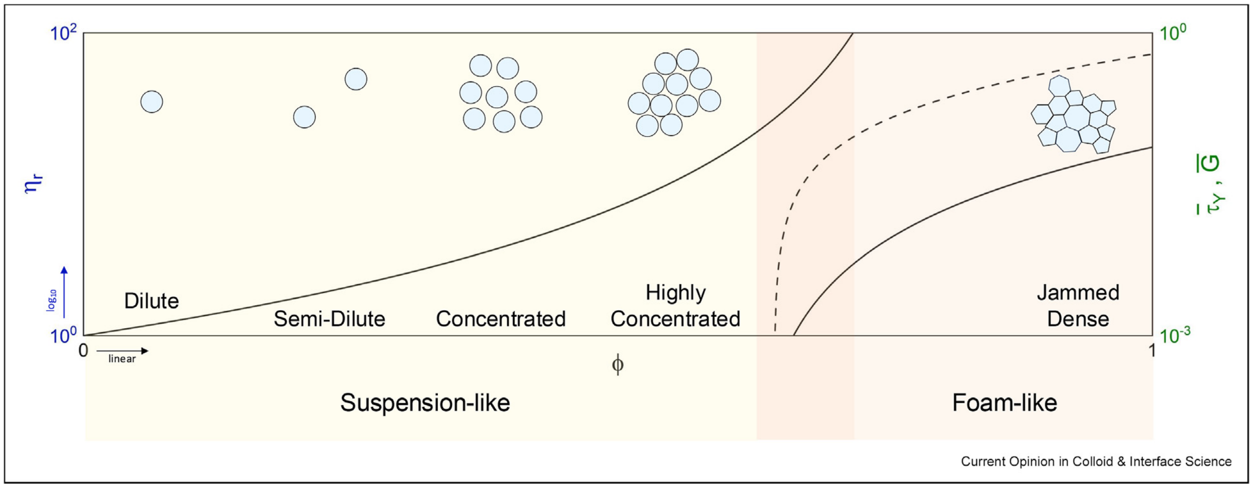

Current Opinion in Colloid & Interface Science

Emulsion rheology and microstructure as a function of dispersed-phase volume fraction. Representative curves show the increase in relative viscosity from dilute to highly-concentrated emulsions, and the increase in elastic modulus (dashed line) and yield stress (continuous line) for jammed dense emulsions. The viscometic properties of dilute to highly-concentrated emulsions as a function of dispersed-phase volume fraction ϕ display analogy with corresponding variation in the microstructure and rheology of deformable particle suspensions. The jammed dense emulsions include polygonal drops and a network of films that contribute to their rheological response. Both elastic modulus and yield stress are normalized by a characteristic capillary stress σ/a.

emulsions [9–12,14,15,58–60]. In 1906, Einstein connected the microhydrodynamics calculation of the flow around dispersed particles to the estimation of viscosity of a dilute suspension of hard spheres [61,62]. Subsequently, Taylor (1932) first analyzed drop deformation in the presence of flow [11] and generalized Einstein's theory [61,62] to describe the viscosity of dilute emulsions by accounting for internal circulation. Decades later, Schowalter, Chaffey, and Brenner (1968) [13] extended the model to suggest the existence of normal stress components, but their model reveals no viscosity variation due to drop deformation. Frankel and Acrivos (1970) [15], and Barthès-Biesel and Acrivos (1972) [63] developed constitutive equations for dilute emulsions that describe the response to transient flows. Choi and Schowalter (1975) [16] carried out the extension to semidilute solutions, whereas Princen and Kiss (1980s) [41] showed the connection between yield stress or elastic modulus and surface tension for dense emulsions and foams. Flumerfelt (1980) first examined the influence of interfacial tension variation as well as dilatational and shear interfacial viscosity on drop deformation in the small deformation limit [21]. Later, Leal, Stone, and coworkers performed a more extensive examination in the limit of large deformation, including the influence of surfactants [18,20,31,59,64].

Barthès-Biesel (1980) began the examination of the deformation and rheology of capsules, defined as viscous drops covered with elastic membranes, and showed that the combination of liquid-like interior enclosed within a solid-like shell leads to rheological properties that cannot be inferred from the rheology of suspension of hard spheres or emulsions containing drops with Newtonian interfaces [65–68]. Oldroyd (1954, 1955) [12,69] presented the first attempt to describe the rheology of nondilute emulsions by adopting the effective medium theory proposed in 1946 by Fröhlich and Sack for the dispersion of deformable particles [70]. Oldroyd also introduced a tensorial framework to capture the complex viscoelastic response of emulsions with appropriate attention to frame invariance. Starting with Taylor's discussion of drop deformation [11] or with Oldroyd's framework [12,69], a large number of analytical and continuum models have emerged, which incorporate the interplay of drop deformation, interactions, breakup, and coalescence processes and rely on numerical and computational approaches, especially for connecting the microstructure and rheology of nondilute and dense emulsions. We provide a selective (and incomplete) but pragmatic overview of the theoretical framework necessary for modeling emulsion rheology.

Scope of this review We provide a brief synopsis of the small-deformation theories based on perturbation methods that are used to capture drop deformation and the rheological response of dilute emulsions to viscometric flows. As dilute emulsions contain noninteracting drops, their shear rheology response under weak flows can be computed both analytically and computationally by adding the contributions from mildly perturbed drops to those by the suspending fluid [9,13–16,59,60,71–78]. We organized the discussion according to the composition of the droplet interface, with detailed discussion of surfactant-free clean drops and surfactant-covered coated drops (modeled as droplets with surface viscosity). Quantitative descriptions of the rheological response for nondilute emulsions rely on supplementing analytical theories with computational fluid dynamics to determine the contributions from the deformation and dynamics of noninteracting or interacting drops and molecular aspects that control the interfacial properties. We tabulate different computational methods and highlight their key findings. As the macroscopic rheological response of emulsions is often compared with the expectations based on constitutive models developed for suspensions of undeformable particles, we include suitable references for completeness [4–7,54,61,62].

In this opinion, we exclude discussions relevant to emulsification and highly nonlinear flows of emulsions [33–35]. We briefly mention the influence of viscoelastic interfaces, drops, or suspending liquids on the emulsion rheology and for the sake of brevity, highlight articles and reviews that detail recent progress and open questions [1,9,20,45,79,80]. Likewise, we exclude studies on capsule suspensions [67,68], wall effects, and the influence of external force fields on droplet topology and emulsion microstructure [45,81–87]. We cite a paucity of datasets and the immensity of challenges involved in theoretical and experimental studies of the extensional rheology response as a reason for excluding a detailed exposition of the few published studies, including our own [26,28,88,89]. We do not cover studies on Pickering emulsions, water-in-water emulsions, microemulsions, and nanoemulsions, and recommend some recent reviews [1,49–51,90,91]. We exclude any discussion of rheometry techniques and measured rheological response of emulsions or interfaces enriched with adsorbed species, but we anticipate that the references included here can be used as a guide for the road not taken [1–5,8,19–23,92–95]. Although capillary pressure, interfacial rheology, disjoining pressure (contributed by intermolecular and surface forces), and bulk rheology of two liquids all influence drainage flows in thin liquid films that separate any droplet pairs and therefore influence emulsion stability and rheology, a comprehensive description of these remains an open challenge [1,8,53,96]. However, we plan to highlight reviews, monographs, articles, and textbooks that form essential reading for appreciating the state-of-the-art understanding and progress in experimental, theoretical, and computational studies of emulsion rheology [3,4,8–10,18-23].

Emulsion microhydrodynamics: the governing equations and scaling

Governing equations and boundary conditions

Emulsions are structured two-phase fluids composed of droplets of density $\rho + \Delta\rho$ and viscosity $\lambda\mu$ suspended in a continuous-phase fluid of density ρ and viscosity μ. If both the dispersed and the continuous phases are Newtonian, incompressible fluids, and the interface is also Newtonian and slip or dissipation free, the only additional material parameter needed is the interfacial tension between the two chosen liquids. In the continuum limit, and in the absence of body-force torques, the linear momentum and mass conservation equations are

$$Re\left(\frac{\partial \mathbf{u}}{\partial t} + \mathbf{u}\cdot\nabla\mathbf{u}\right) = \nabla\cdot\mathbf{\Sigma} \qquad \nabla\cdot\mathbf{u} = 0, \tag{1}$$

where $\mathbf{u}$ is the velocity field averaged over a continuum volume of fluid, $\mathbf{\Sigma}$ is volume-averaged stress tensor in the emulsion, and $Re = uL/\nu$ is the macroscopic Reynolds number defined as ratio of convective to diffusive velocity (or ratio of inertial to viscous stress) [38]. Here we are assuming that variations of an emulsion macroscopic flow occur over a characteristic length scale L, such that $a/L \ll 1$, where a is the average, undisturbed droplet size. Even if both phases exhibit Newtonian flow behavior, the emulsion can exhibit non-Newtonian rheological behavior (e.g., shear thinning and normal stress differences) due to the interplay of droplet-level deformation and relaxation, interfacial dynamics, and interdrop interactions leading to an anisotropic emulsion microstructure in response to imposed bulk stresses [97].

In most applications where emulsions play a key role, droplet size is within the few nanometer to few micron scale such that the local Reynolds number defined in terms of the local shear rate and particle size is $Re_{local} = Re(a/L)^2$ provided that $a/L \ll 1$. Hence, the microhydrodynamics at the droplet level are governed by the low-Reynolds-number flow equations,

$$\mu\nabla^2\mathbf{u} - \nabla p + \rho\mathbf{g} = 0; \quad \nabla\cdot\mathbf{u} = 0 \tag{2}$$

$$\lambda\mu\nabla^2\mathbf{u}' - \nabla p' + (\rho + \Delta\rho)\mathbf{g} = 0; \quad \nabla\cdot\mathbf{u}' = 0 \tag{3}$$

where the primes denote quantities associated with the drop phase, $\mathbf{g}$ is the gravitational acceleration, and p is the mechanical pressure. Equations (2) and (3) are valid everywhere except at the droplet interface denoted by S. Often, models assume that the suspending liquid is density matched with the droplet or dispersed phase.

Boundary conditions encompass, typically, an imposed flow field

$$\mathbf{u} \rightarrow \mathbf{u}^{\infty} \quad \text{as} \quad |\mathbf{x}| \rightarrow \infty, \tag{4}$$

where $\mathbf{x}$ is the position vector measured from the droplet center. At the droplet interface, the Navier-slip condition can be used

$$\mathbf{u} - \mathbf{u}' = \alpha(\mathbf{I} - \mathbf{nn}) \cdot (\mathbf{T} \cdot \mathbf{n}) \quad \text{for} \quad \mathbf{x}_S \in S, \tag{5}$$

where $\mathbf{T}$ is the local Newtonian stress tensor, and $(\mathbf{I} - \mathbf{nn}) \cdot (\mathbf{T} \cdot \mathbf{n})$ is the tangential component of the stress vector $\mathbf{T} \cdot \mathbf{n}$ at the interface. Here $\mathbf{x}_S$ is a point at the droplet surface, and α is a slip coefficient that takes on finite values if interfacial slip occurs. Generally, the velocity at the interface is continuous and $\alpha = 0$ (no slip condition). The traction jump at the interface is given by

$$[\mathbf{n} \cdot \mathbf{T}]_S = (2H\sigma + \Delta\rho \mathbf{g} \cdot \mathbf{x})\mathbf{n} - \nabla_S \sigma \quad \text{for} \quad \mathbf{x}_S \in S, \tag{6}$$

where $[.]_S$ denotes a jump of the bracketed quantity across the interface, $\nabla_S = (\mathbf{I} - \mathbf{nn}) \cdot \nabla$ is the surface gradient operator, and σ is the interfacial tension coefficient which may vary along the droplet interface in response to gradients in temperature or in-homogeneous distribution of surfactant molecules. The mean curvature H is computed using

$$H = \frac{1}{2} \nabla_S \cdot \mathbf{n} \tag{7}$$

In such cases, an equation of state and an evolution equation for surfactant concentration, Γ, are needed for closure [98,99]. Several adsorption isotherms that outline how surface tension varies with change in interfacial concentration of surfactants can be used. We direct the interested reader to Table 1 of Ref. [100] for a comprehensive list. Here, we illustrate the methodology using the non-linear Langmuir equation of state,

$$\sigma(\Gamma) = \sigma_0 + RT\Gamma_\infty \ln\left(1 - \frac{\Gamma}{\Gamma_\infty}\right), \tag{8}$$

where σ_0 is the surface tension of the clean (surfactant-free) interface, R is the ideal gas constant, T is the absolute temperature, and Γ_∞ is the maximum packing concentration of surfactant molecules in a monolayer. In the absence of flow, and after surfactant adsorption occurs for a sufficient time, a steady state interfacial concentration is achieved and an equilibrium surface tension σ_{eq} can be measured. Using this value, the equilibrium surface pressure $\Pi_{eq} = \sigma_0 - \sigma_{eq}$ is defined for a given equilibrium surfactant concentration, Γ_{eq} [101]. The ratio $\Gamma_{eq}/\Gamma_\infty$ known as surface coverage captures the fraction of the interface covered with surfactants.

In the limit of dilute bulk concentration of surfactants, if the adsorption kinetics, and bulk surfactant diffusion are slow compared to local-convective-flow time scales, the surfactant layer at the interface is approximately insoluble and follows a time-dependent convection-diffusion equation [102],

$$\frac{\partial \Gamma}{\partial t} + \nabla_S \cdot (\Gamma \mathbf{u}_S) - D_S \nabla_S^2 \Gamma + 2H\Gamma(\mathbf{u} \cdot \mathbf{n}) = 0, \tag{9}$$

where $\mathbf{u}_S = (\mathbf{I} - \mathbf{nn}) \cdot \mathbf{u}$ is the tangential component of velocity at the interface, and D_S is the surfactant interfacial diffusivity. The second term in Eq. (9) represents surface convection, the third indicates surface diffusion, and the last represents surface dilution due to local changes in interfacial area or surface dilatation.

The evolution of the droplet interface is captured by the kinematic boundary condition,

$$\frac{d\mathbf{x_s}}{dt} = \mathbf{n}(\mathbf{u} \cdot \mathbf{n}). \tag{10}$$

Relevant physicochemical parameters, scales, and dimensionless groups

A characteristic length scale for describing deformation, breakup, or coalescence of drops, is the undeformed drop size, a. A possible characteristic time scale can be defined in terms of the capillary relaxation time or shape relaxation time, written as:

$$\tau_\sigma = \mu a / \sigma_{eq}, \; or \; \tau_\sigma = \lambda \mu a / \sigma_{eq}, \tag{11}$$

As the larger of the two viscosities determines the time period for shape relaxation, the characteristic time scale for $\lambda \gg 1$ is defined as $\tau_\sigma = \lambda\mu a/\sigma_{eq}$ [15,32]. Otherwise $\tau_\sigma = \mu a/\sigma_{eq}$ is typically used, and τ_σ, also called visco-capillary time, captures the time required to traverse a distance comparable to drop size, with an intrinsic capillary velocity, σ_{eq}/μ set by the ratio of two physicochemical parameters or material properties: interfacial tension and viscosity [38]. The two material parameters can be used to estimate the characteristic scale for pressures or stresses, as follows. The ratio σ_{eq}/a, provides an estimate for capillary stress, whereas $\mu\dot{\gamma}$ estimates the viscous stress.

Assuming a neutrally-buoyant drop ($\Delta\rho = 0$) in an imposed linear flow field where $\mathbf{u}^\infty \sim \mathbf{x} \cdot \nabla \mathbf{u}$, the characteristic time scale for the flow is $\tau_f = \dot{\gamma}^{-1}$, where $\dot{\gamma}$ is the magnitude of the local velocity gradient. A typical timescale for droplet deformation in shear is $\tau_d \sim \tau_f = \dot{\gamma}^{-1}$. Setting the undeformed drop size, a, as the characteristic length scale, a natural choice for the characteristic velocity is $\dot{\gamma}a$ and hence, from Eqs. (2) and (3), the pressures inside and outside of the droplet scale as $\mu\dot{\gamma}$ and $\lambda\mu\dot{\gamma}$, respectively. The choices of characteristic time, length, and stress/pressure scales determine the form of dimensionless equations and boundary conditions obtained after a nondimensionalization of Eqs. (2)−(10).

The dimensionless ratio of viscous and capillary stresses is defined as the capillary number

$$Ca = \frac{\mu\dot{\gamma}}{\sigma_{eq}/a} = \frac{\dot{\gamma}a}{\sigma_{eq}/\mu} = \frac{\tau_\sigma}{\tau_d}. \tag{12}$$

Alternatively, Ca equals the ratio of imposed flow velocity, $\dot{\gamma}a$ to intrinsic capillary velocity, σ_{eq}/μ. The capillary number can be written equivalently as the ratio of capillary relaxation time to deformation time. Since Ca is also a product of relaxation time, τ_σ and deformation rate ($\dot{\gamma}$ for shear), it captures the flow strength in a fashion reminiscent of Weissenberg number $Wi = \dot{\gamma}\tau_1$ used in polymer rheology, with τ_1 representing the longest relaxation time. Thus, Ca captures the relative magnitude of stress, velocity, and flow strength for calibrating the influence of applied flow conditions on drop deformation and dynamics. Again, for $\lambda \gg 1$, the Ca values should be computed by considering $\tau_\sigma = \lambda\mu a/\sigma_{eq}$ as the shape relaxation time [15,32].

Two additional dimensionless groups are written as the ratio of stresses or pressures. The Bond number, Bo captures the ratio of hydrostatic to capillary pressures, relevant to determining buoyancy-driven motion and the influence of gravity on the shape and deformation of drops. The Marangoni number, Ma, is a ratio between restoring Marangoni stresses $\Delta\sigma/a$ that arise due to surface tension variation, $\Delta\sigma$ and distorting viscous stresses,

$$Bo = \frac{\Delta\rho g a}{\sigma_{eq}/a}, \quad Ma^{-1} = \frac{\mu\dot{\gamma}}{\Delta\sigma/a}. \tag{13}$$

If the origin of the Marangoni stress is a nonuniform surfactant contribution, then the characteristic magnitude of surface-tension variation equals the magnitude of surface compression modulus $\Delta\sigma = -\Gamma_{eq}(\partial\sigma/\partial\Gamma)_{\Gamma=\Gamma_{eq}}$ that arises from perturbations about the equilibrium surface concentration, Γ_{eq}. The dimensionless ratio of $\Delta\sigma$ to σ_{eq} represented by β is a surface elasticity parameter [74,77],

$$\beta = \frac{\Delta\sigma}{\sigma_{eq}} = CaMa, \quad Pe_S = \frac{\dot{\gamma}a^2}{D_S}, \tag{14}$$

where, Pe_S is the surface Péclet number denoting the relative balance between surfactant convection and diffusion along the interface. Modeling emulsification by mechanical methods [33,34,103,104] can sometimes require the evaluation of inertial effects using the characteristic inertial pressure estimated as ρU^2. For example, the Reynolds number, $Re = \rho U^2/(\mu U/a)$ and Weber number, $We = \rho U^2/(\sigma/a)$ are defined as the ratio of inertial pressure to viscous and capillary stress, respectively [38].

Dissipative effects due to shear and dilatational surface viscosity may affect the dynamics of droplets in flows [20]. Two dimensionless Boussinesq numbers that capture the interplay between bulk viscous stresses and dissipative interfacial stresses, are defined as

$$Bq_s = \frac{\mu_s}{\mu a}, \quad Bq_d = \frac{\mu_d}{\mu a} \tag{15}$$

for shear surface viscosity, μ_s, and dilatational viscosity, μ_d, respectively. In such cases, the right-hand side of the traction jump boundary condition in Eq. (6) is augmented by an additive interfacial-viscous traction of form, $\nabla_S \cdot \tau_S$, obeying the deviatoric part of the Boussinesq-Scriven constitutive law for Newtonian interfaces [19,95,105,106],

$$\boldsymbol{\tau}^s = 2\mu_s\mathbf{E}_s + (\mu_d - \mu_s)(\mathbf{I}_S : \mathbf{E}_S)\mathbf{I}_S, \tag{16}$$

where $\mathbf{E}_S = \frac{1}{2}\left[\nabla_S\mathbf{u}\cdot\mathbf{I}_S + \mathbf{I}_S\cdot(\nabla_S\mathbf{u})^T\right]$ is the surface rate of deformation tensor, and $\mathbf{I}_S = \mathbf{I} - \mathbf{nn}$ is a surface projector tensor. Consistent with the traction jump in Eq. (6), normalizing Eq. (16) by a characteristic surface stress $\mu\dot{\gamma}a$, characteristic length a, and velocity $\dot{\gamma}a$ yields the dimensionless Boussinesq numbers in Eq. (15).

Incorporating surface viscosity can alter the interfacial force balance in Eq. (6) and interfacial transport of surface-active entities at complex interfaces. Gradients in surface tension ($\nabla_S\sigma$) generate Marangoni stresses. Interfacial shear viscosity characterizes the resistance to interfacial shear flow, and surface dilatational viscosity captures the resistance to dilatational effects that can influence coalescence [60,107–109]. Interfacial concentration and interaction between adsorbed molecules (and macromolecules) influence interfacial tension, σ and surface pressure, $\Pi = \sigma_0 - \sigma$ that depend on the surface tension reduction compared to value at a clean interface, σ_0.

Several studies suggest that surface viscosity depends exponentially on surface pressure [100,110–113].

$$\mu_i = \mu_{i,eq}\exp\left(\frac{\Pi - \Pi_{eq}}{\Pi_c}\right), \tag{17}$$

where $i = s, d$ identify shear and dilatational viscosities, $\mu_{i,eq}$ and Π_{eq} are the equilibrium surface viscosity and surface pressure, respectively, and Π_c is a characteristic scale of surface pressure variations. Positive values of Π_c indicate Π-thickening surfactants, while negative values are used for Π-thinning surfactants. The relation between surfactant transport and surface viscous stresses is given by combining Eqs. (8) and (17) yielding the surfactant-concentration-dependent Boussinesq numbers, defined as follows

$$Bq_i = Bq_{i,eq}\left(\frac{1 - \widehat{\Gamma}_{eq}}{1 - \widehat{\Gamma}}\right)^{\beta/\hat{\Pi}_c}, \tag{18}$$

where $i = s, d$ indicate the type of surface viscosity, $Bq_{i,eq}$ is a reference equilibrium value, $\widehat{\Pi}_c = \Pi_c/\sigma_{eq}$, $\widehat{\Gamma} = \Gamma/\Gamma_\infty$, $\widehat{\Gamma}_{eq} = \Gamma_{eq}/\Gamma_\infty$, and β is the elasticity parameter. Typically, the ratio of dilatational to surface viscosity λ_{ds} is used to study the relative importance of both surface viscosities.

Emulsions of droplets with slip-boundaries have been used to model the rheology of emulsions of immiscible polymer blends, where the slip coefficient is defined by the ratio of the interfacial thickness and some isotropic interfacial viscosity [59,114,115]. Nondimensionalizing Eq. (5) yields a dimensionless slip coefficient $\overline{\alpha} = \alpha/(\mu a)$.

Emulsions with one or both phases as non-Newtonian require additional parameters and considerations, which depend on the choice of the constitutive model made for capturing one or more features typical of non-Newtonian behavior: rate-dependent shear and extensional viscosity, first and second normal stress difference, and relaxation time. Even in the simplest case of the second-order fluid model for both phases, two normal stress differences N_{1i} and N_{2i} each arise for dispersed ($i = d$) and suspending ($i = s$) phases, creating at least four additional dimensionless parameters:

$$N_{1i}a/\sigma_{eq},\ N_{2s}/N_{1s},\ N_{2d}/N_{1d},\ De_i = \tau_i/\tau_\sigma, \tag{19}$$

where $\tau_i = N_{1i}/\Sigma_{12i}$ can be used for defining the relaxation time for suspending or dispersed phase, in which case if we define $\overline{N}_{1i} = N_{1i}a/\sigma_{eq}$ then $De_i = \overline{N}_{1i}/Ca^2$, [9,45,116]. The relaxation time for the viscoelastic fluid phase can be alternatively determined using the linear viscoelastic response measured in oscillatory shear, stress relaxation, dynamic light scattering or capillarity-based extensional rheology, and each response captures aspects of non-Newtonian response that need not correlate directly with the first normal stress difference.

Emulsion macroscopic stress

The continuum, macroscopic volume-averaged stress in Eq. (2) for an emulsion where both dispersed and suspending fluids are Newtonian is

$$\boldsymbol{\Sigma} = \boldsymbol{\Sigma}^0 + \phi\boldsymbol{\Sigma}^p, \tag{20}$$

where ϕ is the drop-phase volume fraction, and $\langle . \rangle$ denote the volume-average of the quantity in brackets. Here $\boldsymbol{\Sigma}^0 = -\langle p\rangle\mathbf{I} + 2\mu\langle\mathbf{E}\rangle$ is the Newtonian stress contribution from the continuous phase. In analogy with a particulate system [117], the extra stress in an emulsion due to the dispersed droplets can be determined using the following expression:

$$\boldsymbol{\Sigma}^p = \frac{3}{4\pi a^3}\frac{1}{N}\sum_{\alpha=1}^{N}\mathbf{S}^\alpha, \tag{21}$$

where the sum accounts for the stress contribution of each one of the N drops in emulsion (or particles in suspension) given by the Landau-Batchelor tensor [118] defined as

$$\mathbf{S}_{ij}^\alpha = \int_S \left[(\Delta\mathbf{f})_i x_j + \mu(\lambda - 1)(u_i n_j + n_i u_j)\right] dS. \tag{22}$$

The Landau-Batchelor tensor depends on the surface traction and the velocity distribution over the particle surface, where local low-Reynolds number conditions hold and no external torques are applied. In the limit of a sharp fluid interface, $\boldsymbol{\Sigma}\cdot\mathbf{n} \rightarrow \Delta\mathbf{f}$ captures the stress jump across the interface defined in Eq. (6). For example, considering clean, neutrally buoyant droplets, $\Delta\mathbf{f} = 2H\sigma\mathbf{n}$.

Thus, the connection between microscopic behavior and macroscopic rheology is embedded in the definition of the macroscopic particle-stress contribution $\boldsymbol{\Sigma}^p$ given by equation Eq. (21). The stress jump across the interface, $\Delta\mathbf{f}$, captures the microscale physics, while $\boldsymbol{\Sigma}^p$ accounts for the contribution of the dispersed phase. The emulsion shear rheology is defined by a shear stress Σ_{12} and first- and second-normal stress differences that arise from contributions of the dispersed phase only, [119].

$$N_1 = \phi N_1^p = \phi(\Sigma_{11}^p - \Sigma_{22}^p), \tag{23}$$

$$N_2 = \phi N_2^p = \phi(\Sigma_{22}^p - \Sigma_{33}^p). \tag{24}$$

Further, relative viscosity, $\eta_r \equiv (\eta/\mu)$ that equals emulsion viscosity η scaled by the suspending fluid viscosity μ can be defined in terms of $\overline{\Sigma}_{12}$the dimensionless form of extra stress due to added particles or drops as given by Eq. (21). Thus, the relative viscosity has the following form

$$\eta_r = 1 + \phi Ca^{-1}\overline{\boldsymbol{\Sigma}}_{12}^p, \tag{25}$$

where

$$\overline{\boldsymbol{\Sigma}} = \frac{\boldsymbol{\Sigma}}{\mu\dot{\gamma}},\quad \overline{\boldsymbol{\Sigma}}^0 = \frac{\boldsymbol{\Sigma}^0}{\mu\dot{\gamma}},\quad \overline{\boldsymbol{\Sigma}}^p = \frac{\boldsymbol{\Sigma}^p}{\sigma_{eq}/a}. \tag{26}$$

Even though both dispersed and suspending fluids are assumed to be Newtonian, experimental, theoretical and numerical simulations show that emulsions can exhibit non-Newtonian response, including shear-thinning and finite normal stress differences ($N_1 > 0$ and $N_2 < 0$). The surface-tension-driven recovery or relaxation of the perturbed drop shape to the minimum surface area for a fixed volume underlies the origin of viscoelasticity. The ratio of this shape relaxation time $\sim \mu a/\sigma_{eq}$ to imposed flow rates $\dot{\gamma}^{-1}$ is a dimensionless group, defined as Ca in Eq. (12) that evokes the Weissenberg number, Wi in elastic soft materials, and likewise, a nonlinear response is observed for $Wi > 1$. Equations (20)−(25) hold for the analysis of dilute to concentrated suspensions. Polydispersity in drop sizes of emulsions can be included in the derivation of Eq. (20) if the distribution of drop sizes is known. At higher concentrations, near the maximum volume fraction of drops, more elaborate constitutive equations are needed to adequately capture the rheological response of the emulsions. The stress and flow behavior of the jammed dense emulsions are discussed in the section titled Jammed dense emulsions with polygonal drops in a network of films.

Dilute emulsions: small deformation theory and constitutive models

In this section, we summarize key features of theoretical and numerical investigations of single-drop dynamics and rheology of dilute emulsions by including three cases: clean drops, surfactant-covered drops, and drops with slip at interfaces. We revisit significant theoretical advances made analytically in the two asymptotic limits of small or large droplet deformations in viscometric flows [32,120]. We mention numerical studies used for bridging the gap between the two asymptotic limits for clean drops [73,121,122], surfactant-covered droplets [64,99,123−129], and drops with viscous interfaces [107−109,130−132]. The approaches discussed here form the starting point for investigations on emulsions containing interfaces with non-Newtonian interfacial rheology, or composed of dispersed or suspending fluid with a non-Newtonian rheology response. For example, proteins or particles as emulsifiers can lead to significant interfacial viscoelasticity [133] or interfacial yield stress, and the presence of lipid membranes and protein gel networks at interface can create bending and elastic moduli manifested in suspensions of vesicles and cells, including blood. We recommend recent reviews and papers for discussions of emulsions containing complex interfaces that exhibit non-Newtonian interfacial rheology or emulsions formed by using a non-Newtonian dispersed or suspending fluid [1,9,45].

Small deformation of drops in shear and extensional flows

Taylor's deformation parameter In 1932, Taylor generalized Einstein's formula for viscosity of a dilute suspension of hard spheres to derive an expression for the viscosity of dilute emulsions in the limit of low Ca, clean interface droplets, and for cases with Newtonian dispersed and suspending fluids. The expression for relative viscosity, $\eta_r = (\eta/\mu)$ in the limit of low shear rate (or low Ca) is given by

$$\eta_r = 1 + \frac{5}{2}\phi\frac{(\lambda + 2/5)}{(\lambda + 1)} = 1 + \frac{5}{2}\phi g_T(\lambda), \qquad (27)$$

where $g_T(\lambda) = (\lambda + 2/5)/(\lambda + 1)$ is Taylor's viscosity factor. Recalling that the specific viscosity $\eta_{sp} = (\eta_r\text{-}1)$ equals the ratio of the contribution of dispersed and suspending phases to viscosity, we deduce, from Taylor's expression, an alternative form for specific viscosity of emulsions,

$$\eta_{sp}\big/\phi = \mathbf{\Sigma}^p_{12}\big/\mu\dot{\gamma} = \frac{5}{2}g_T(\lambda). \qquad (28)$$

In the limit of a large λ, Taylor's viscosity factor goes to unity or $g_T(\lambda) = 1$ recovering the Einstein's formula for suspensions. Upon defining the specific viscosity as $\eta_{sp} = (\eta_r\text{-}1)$, Eq. (27) yields $\eta_{sp} = (5/2)\,\phi g_T(\lambda)$. In the limit of vanishingly small λ, the parameter $g_T(\lambda) \rightarrow 2/5$, implying the relative viscosity of bubbly fluid is just $\eta_r = 1 + \phi$ and the specific viscosity of bubbly fluid is $\eta_{sp} = \phi$.

Taylor [11,134] was the first to theoretically and experimentally study the deformation of a neutrally buoyant viscous drop in response to imposed shear or extensional flows, and describe how bulk rheology is informed by drop deformation and orientation at the microscopic scale. For a weakly perturbed spherical drop, the shape change can be measured using a scalar quantity called Taylor's deformation parameter defined as

$$D_T = \frac{L - B}{L + B}, \qquad (29)$$

where L and B are the major and minor axes of the ellipsoid projected onto the velocity-shear rate plane, as shown in Figure 2. For large deformations, especially those encountered in response to extensional flows, L/B is usually used instead of D_T [120]. According to Taylor, at steady state, the small deformation of a clean droplet in response to weak shear flows [134], exhibits

$$D_T = \frac{(19\lambda + 16)}{(16\lambda + 16)}Ca + O(Ca^2) = d_T(\lambda)Ca + O(Ca^2). \qquad (30)$$

Here, for brevity's sake, we define the viscosity ratio-dependent prefactor as the Taylor's deformation prefactor $d_T = (19\lambda + 16)/(16\lambda + 16)$.

Inclination or orientation of deformed drops In flows with a rotational component of velocity including viscometric shear flows, the ellipsoidal drop (or ellipsoid projection of the deformed drop) orients. An inclination angle, θ can be measured between the major axis of deformation and the flow direction, as shown in Figure 2. Chaffey and Brenner [58] computed the inclination angle exhibited by perturbed drops in weak flows by

Figure 2

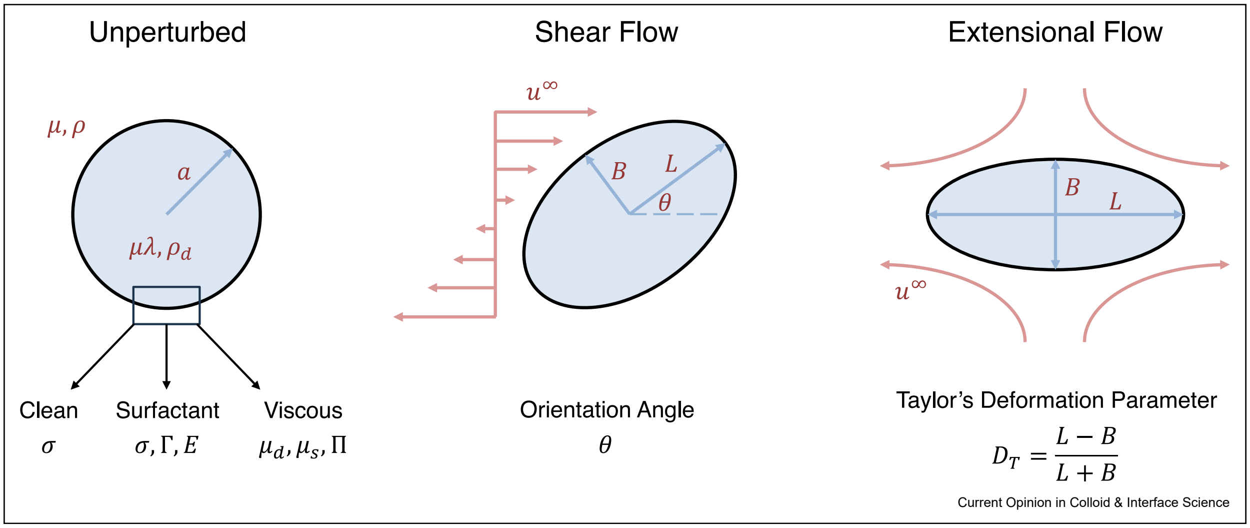

Representative drop deformation in shear and extensional flows is characterized in terms of orientation angle and deformation parameter. The unperturbed shape added as a references highlights interfacial properties: interfacial tension, σ, interfacial concentration, Γ, surface pressure, Π, surface compressional modulus (or Gibbs modulus), $E = -A(\partial\Pi/\partial A)$, dilatational viscosity, μ_d and interfacial shear viscosity, μ_s relevant for clean, surfactant-laden and viscous interfaces. Additional parameters are required for viscoelastic and viscoplastic interfaces.

carrying out perturbation analysis up to second order in Ca, leading to the following expression

$$\theta = \frac{\pi}{4} - \frac{(2\lambda+3)}{5}\frac{(19\lambda+16)}{(16\lambda+16)}Ca + O(Ca^2), \tag{31}$$

or

$$\theta = \frac{\pi}{4} - \frac{d_T}{c_0}Ca + O(Ca^2), \tag{32}$$

where $c_0(\lambda) = 5/(2\lambda+3)$. In dilute emulsions, the flow-induced droplet dynamics depend on the physicochemical properties of the two liquids (density and viscosity), composition-dependent properties of the interface (interfacial tension, interfacial rheology, and surface forces), and the strength and type of imposed flow fields (shear and extensional). Qualitatively, the extent of drop deformation and orientation for clean droplets is influenced by an interplay of viscous and capillary stresses dependent on Ca, appropriately defined by accounting for interfacial tension, deformation rate, and viscosity ratio λ ranging from 0 to ∞.

Clean droplet dynamics In weak flows, $Ca \ll 1$, steady shapes are nearly spherical, and the inclination angle $\theta \sim 45°$, to leading order in Ca, as sketched in Figure 2 and first analyzed and visualized by Taylor [134]. For the two extreme values of λ i.e. 0 and ∞, the deformation prefactor, d_T ranges between 1 and 1.187, implying that in weak flows, the drop deformation parameter D_T is linearly dependent on Ca. The inclination, θ according to Chaffey and Brenner equation (32) shows a linear dependence on Ca. Visualizing drop deformation under mild flow provides a means of measuring interfacial tension, even when the interfacial tension is extremely small, for example, in water-in-water emulsions or in coacervates. Alternatively, the relaxation of a perturbed drop to its unperturbed state after cessation of flow can be used to measure shape relaxation time and interfacial tension. At higher flow strengths, for a given λ, droplet shape becomes more elongated as Ca increases, and the major axis of deformation aligns with the flow direction as the droplet rotates in response to the local vorticity of the flow. In this limit, drops with viscosities below a critical value $\lambda_c \sim 4$ may undergo breakup at a critical flow strength Ca_c, whereas high-viscosity drops remain stable for $\lambda > \lambda_c$, for arbitrary Ca [32,120]. For example, clean droplets with the same viscosity as the suspending medium undergo breakup at a critical value $Ca_c \approx 0.43$ [135].

Experiments by Mason and coworkers [29,136] characterized the transient and equilibrium drop shapes for $\lambda < \lambda_c$ and observed breakup modes for clean droplets as illustrated by cases reproduced in Figure 3(a). Breakup modes were observed to depend on a balance between the rate of increase of capillary number up to and across Ca_c and the shape relaxation time. For $\lambda < 0.2$ and high Ca rates, the droplets experience tip-streaming breakup mode; whereas for low enough Ca rates, tip-streaming breakup may be suppressed and the droplet deforms

Figure 3

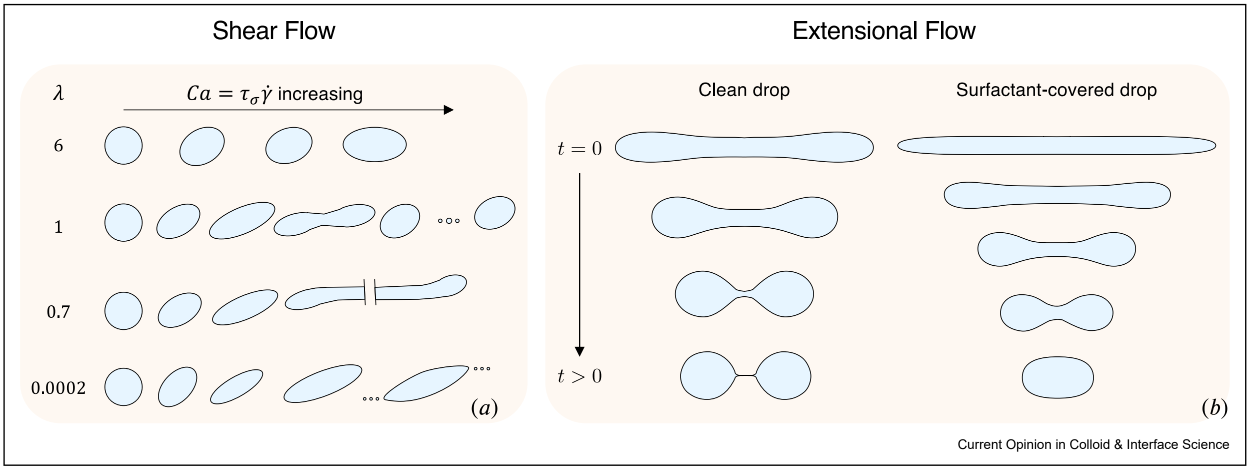

Schematic diagram of droplet deformation in shear and extensional flows. Image adapted from Ref. [136] for shear flow experiments (a) and from figure 9 in Ref. [123] for numerical results in extensional flows (b). The two sets in extensional flows depict snapshots of drop relaxation of clean and surfactant-covered droplets at different dimensionless times as indicated. Details on the experimental data sets in part (a) are listed in Appendix C.

into a thin-liquid thread and breakup into smaller droplets by Rayleigh instability. However, numerical and experimental results in extensional flows support the assumption that tip-streaming instabilities occur only in the presence of surfactants [31,109,124,137]. Theoretical and numerical analysis on tip-streaming breakup instability remains an active area of research.

In weak extensional flows, clean droplets attain a stable, stationary shape for all λ, where the droplet principal axis of deformation is aligned with the flow direction of maximum extension, as illustrated in Figure 3(b), adapted from Milliken et al. [123]. Here, the transient approach to steady shapes is monotonic, since the flow is vorticity-free. For $Ca = O(1)$, two main regimes of droplet steady deformation are of interest: (i) nearly ellipsoidal shapes are observed for moderate and large λ, (ii) for $\lambda \lesssim 0.1$, droplets deform into shapes with nearly-pointed ends. For larger values of Ca, high-viscosity drops deform into slender threads that eventually break up into smaller droplets. Low-viscosity drops are able to sustain highly elongated shapes for even larger flow strengths, but will break up into small droplets via Rayleigh-Plateau instability if $Ca \gg Ca_c$. Drop relaxation after the flow field is switched off may also lead to drop breakup into a chain of droplets of uniform size if the droplet's initial shape is sufficiently elongated by the flow.

Deformation of coated droplets The presence of surface inclusions (e.g. surfactant molecules, proteins, and lipids) alters the classical dynamics of transient and steady shapes of clean droplets [20]. For surfactant-covered drops, deviations from the clean droplet deformation are governed by a balance among (i) interface convection of surfactants towards regions of high curvature and stagnation points lowering surface tension locally, (ii) local surfactant dilution due to drop deformation and creation of surface area, and (iii) diffusion of surfactant, which tends to homogenize the surfactant distribution along the interface. Gradients in surface tension induce Marangoni stresses, which act against surface deformation [21,60,64]. The critical Ca_c for the onset of unsteady deformation and breakup is usually larger compared to clean droplet results, but it can be smaller depending on flow strength and on the local vorticity of the flow [74].

Figure 3(b) shows the relaxation of clean and surfactant-covered droplets at different times after being initially deformed by an extensional flow. Surfactant redistribution along the droplet surface stabilizes the shape against transient configurations that may lead to droplet breakup. The qualitative behavior of droplets with viscous interfaces in linear flows introduces an additional surface viscous stress to the force balance Eq. (6), where droplet shape and rheology depend on flow type and emulsion's composition, for example, the relative contribution of shear and dilatational surface viscosities and their relation to surface pressure and surface tension [60,108,130,132]. Thus, droplets may attain steady shapes or undergo transient flow-induced deformation, possibly leading to interfacial instabilities and breakup (e.g. tip-streaming, burst, and thread breakup by Rayleigh instability) [29,32,120,138].

Deformation of a drop in an emulsion with non-Newtonian component(s) The deformation of drops in emulsions containing one non-Newtonian phase have received more attention than the cases with both non-

Newtonian phases. Experiments, analytical theory and numerical simulations show that viscoelasticity changes both the drop deformation and Ca_c above which elongated drops break up. A detailed understanding of the interplay of capillarity and viscoelasticity is absent even for drop coalescence and breakup as it requires examination and understanding of the influence of rate-dependent shear viscosity, transient and steady extensional viscosity, normal stress differences, and for polymeric fluids, finite extensibility and non-Hookean elasticity [27,45,116,139–143]. The experimentalists often utilize constant-viscosity elastic fluids called Boger fluids to isolate the effect of elasticity without interference from rate-dependent viscosity behavior. The constant viscosity elastic fluids can be considered analogs of Oldroyd-B fluids especially, while modeling shear rheology response, and for the small deformation case, the simpler second-order fluid model provides a reasonable starting point [9,116]. However, these models are suitable for comparisons with experiments only for slow flows, but the practical problems of dilute and nondilute emulsions often require an understanding of response to strong flows and coupling between rate-dependent viscous and nonlinear viscoelastic effects [9,45,116].

We recommend the classical papers by Leal's group for a comprehensive survey of clean droplet dynamics in unbounded shear and extensional flows [30,31], including studies when dropping or suspending fluid is non-Newtonian [142–144]. We direct the interested readers to Guido's review on droplet deformation in confined flows and viscoelastic fluids [45]. Numerical methods used for visualization of drop deformation in nondilute emulsions for different choices of λ, flow types, Ca, interfacial properties, and Newtonian or viscoelastic fluids are summarized in a later section. Next we describe how drop deformation, orientation, and shape relaxation provide ingredients for deriving or prescribing constitutive models for emulsions by incorporating the role of interfacial and bulk properties of dispersed and suspending fluids.

Constitutive models for dilute emulsions

Evolution of the shape distortion tensor In the limit when a suspended, neutrally buoyant, clean droplet of undeformed, spherical radius a deviates from sphericity to slight ellipticity, the perturbed drop shape [14,15,88] is described by the following expression:

$$S(t) = r(t) - a\left(1 + \epsilon \frac{\mathbf{x}\cdot\mathbf{A}(t)\cdot\mathbf{x}}{r^2}\right) + O(\epsilon^2) = 0, \qquad (33)$$

where $\epsilon \ll 1$ is a perturbation parameter, and $r = (\mathbf{x}\cdot\mathbf{x})^{1/2}$. The shape distortion tensor, $\mathbf{A}$, measures the droplet deformation embedded in the current configuration relative to a reference configuration. The components of $\mathbf{A}$, a second-order tensor, are determined in terms of a second-order deformation gradient tensor, $\mathbf{F}$, that maps the deformation of the material lines from reference to current configuration [145]. Please refer to Appendix A for a more detailed description.

The rate of change in the droplet shape depends on the kinematics of the imposed flow $\mathbf{u}^{\infty} = (\mathbf{E}+\mathbf{W})\cdot\mathbf{x}$, and thus on the rate-of-strain tensor $\mathbf{E}$ and vorticity tensor $\mathbf{W}$. The distortion tensor $\mathbf{A}$ can be used to calculate the Taylor deformation parameter D_T, orientation (inclination angle in shear flows) and define rheological material properties of the emulsion. The evolution of the distortion tensor in a reference frame that translates and rotates with the droplet [32,78] is captured by the following expression

$$\epsilon\frac{\partial \mathbf{A}}{\partial \bar{t}} - Ca\overline{\mathbf{W}}\cdot\epsilon\mathbf{A} + \epsilon Ca\mathbf{A}\cdot\overline{\mathbf{W}} = Ca\, c_0(\lambda)\overline{\mathbf{E}} \\ - c_1(\lambda)\epsilon\mathbf{A} + O(\epsilon Ca, \epsilon^2). \qquad (34)$$

Here, the two coefficients $c_0(\lambda) = 5/(2\lambda + 3)$ and $c_1(\lambda) = 40(\lambda+1)/[(19\lambda+16)\ (2\lambda+3)]$ depend primarily on viscosity ratio, λ. The coefficient $c_0(\lambda)$ appeared in the definition of the deformation parameter, D_T in Eq. (32). The dimensionless quantities are defined for time, strain rate tensor and vorticity tensor, respectively, as $\bar{t} = t/(\mu a/\sigma)$, $\overline{\mathbf{E}} = \mathbf{E}/\dot{\gamma}$, $\overline{\mathbf{W}} = \mathbf{W}/\dot{\gamma}$, and $|\mathbf{A}| = 1$. A derivation of Eq. (34) is included in the Appendix A for completeness. The right-hand side of Eq. (34) captures how the rate of change of $\mathbf{A}$ is contributed by two competing terms. The first term distorts away from a spherical shape and is linearly dependent on the rate of strain, whereas the second term restores unperturbed shape and depends on $\mathbf{A}$. The neglected terms of $O(\epsilon^2)$ correspond to harmonics higher than second, whereas terms of $O(\epsilon Ca)$ arise from the straining flow acting on the distorted shape [32]. It is possible to rewrite $c_1(\lambda) = 1/[2c_0 d_T]$ and reframe the Eq. (34) to appear as:

$$\epsilon\frac{\partial \mathbf{A}}{\partial \bar{t}} - Ca\overline{\mathbf{W}}\cdot\epsilon\mathbf{A} + \epsilon Ca\mathbf{A}\cdot\overline{\mathbf{W}} = Ca\, c_0\overline{\mathbf{E}} \\ - \frac{1}{2c_0 d_T}\epsilon\mathbf{A} + O(\epsilon Ca, \epsilon^2). \qquad (35)$$

The form of Eq. (34) or Eq. (35) reveals two small deformation regimes: (i) for weak flows (i.e. $\epsilon \sim Ca \ll 1$ and $\lambda = O(1)$), the distortion is limited by a strong interfacial tension effect, and (ii) large-λ and arbitrary Ca but not too large for flows with sufficient vorticity where $\epsilon \sim \lambda^{-1} \ll 1$. For a given flow type and small parameter ϵ, Eq. (34) is solved for the distortion tensor $\mathbf{A}$. Here, we summarize up to second-order deformation theories for clean droplet deformation and rheology in viscometric flows and include the results for surfactant-covered drops, interfacially viscous drops and drops with interfacial slip conditions. The interfacial slip case is key to understanding the rheology of polymer blends emulsions formed by phase separation.

Clean droplets in shear flows For a clean droplet in weak shear flows where $\epsilon = Ca \ll 1$ and $\lambda = O(1)$, the deformation parameter D_T derived by Taylor [134] and the inclination angle θ as demonstrated by Chaffey and Brenner [58] shows a linear dependence on Ca. These expressions discussed in the previous section and given by Eqs. (36) and (32), respectively, are reproduced here for clarity of presentation,

$$D_T = \frac{19\lambda + 16}{16\lambda + 16} Ca + O(Ca^2) = d_T Ca + O(Ca^2), \tag{36}$$

$$\theta = \frac{\pi}{4} - \frac{d_T}{c_0} Ca + O(Ca^2). \tag{37}$$

In the other limit when $Ca = O(1)$ and $\epsilon = \lambda^{-1} \ll 1$, the leading order solutions for the Taylor deformation parameter and inclination angle are

$$D_T = \frac{5}{4}\lambda^{-1} + O(\lambda^{-2}), \quad \theta = \frac{10}{19}\frac{\lambda^{-1}}{Ca} + O(\lambda^{-2}). \tag{38}$$

Higher-order theories have been developed; for detailed derivation and formulas, see Refs. [60,77,78,88,146].

For clean drops in shear flows in the weak flow limit when $\epsilon = Ca \ll 1$ and arbitrary λ, a second-order deformation analysis [13,63,77] leads to the following equations that describe the characteristic rheological behavior of dilute emulsions

$$\frac{\Sigma^p_{12}}{\mu\dot{\gamma}} = \frac{5}{2}\, g_T - \frac{4}{5} d_T D_1(\lambda) Ca^2 + O(Ca^3), \tag{39}$$

$$\frac{N^p_1}{\mu\dot{\gamma}} = \frac{32}{5} {d_T}^2 Ca, \tag{40}$$

$$\frac{N^p_2}{\mu\dot{\gamma}} = -\frac{1}{2}\frac{N^p_1}{\mu\dot{\gamma}} - \frac{4}{5} Ca\, d_T D_2(\lambda) \tag{41}$$

where the coefficients D_0 and D_1 are listed in Appendix A.1. Equations (39)—(41) reveal the characteristic shear-thinning behavior of emulsion flows with finite positive first normal stress difference and negative second normal stress difference, respectively.

Since $\Sigma^p_{12}/\mu\dot{\gamma} = \eta_{sp}/\phi$, the explicit use of g_T, d_T and c_0 in writing the contributions of dispersed phase (or particulates) to shear stress, specific viscosity, and normal stress differences provides two key benefits. The expressions appear more compact and allow for clearer comparisons. Also, from λ ranging from zero (bubble) to infinity (rigid particle), d_T varies from 1 to 1.187, whereas $g_T = (\lambda + 2/5)/(\lambda + 1)$ increases from 2/5 to 1.

In the limit when $\epsilon = \lambda^{-1} \ll 1$ for arbitrary λCa, Oliveira & da Cunha [78] developed a second-order perturbation theory in powers of λ^{-1} and showed that

$$\frac{\Sigma^p_{12}}{\mu\dot{\gamma}} = \left(\frac{5}{2} - \frac{25}{4\lambda}\right) + \frac{5}{\lambda}\frac{20/19}{\left[(20/19)^2 + (\lambda Ca)^2\right]}, \tag{42}$$

$$\frac{N^p_1}{\mu\dot{\gamma}} = \frac{10}{\lambda}\frac{(\lambda\, Ca)^2}{\left[(20/19)^2 + (\lambda Ca)^2\right]}, \quad \frac{N^p_2}{\mu\dot{\gamma}} = -\frac{29}{133}\frac{N^p_1}{\mu\dot{\gamma}}. \tag{43}$$

The shear rheology of high-viscosity drops reveals two limits. When $Ca \ll 1$ or weak flows, emulsions of high-viscosity drops behave as Boger fluids with shear rate-independent viscosity and vanishing but finite normal stress differences; a similar behavior is observed for $Ca = O(1)$.

Surfactant-covered drops Vlahovska et al. [77] extended the small-deformation theory for clean droplets to surfactant-covered drops valid for arbitrary viscosity ratios and elasticity parameter. In weak flows, the deformation and inclination angle at leading order are

$$D_T = \frac{5}{4} Ca + O(Ca^3), \tag{44}$$

and

$$\theta = \frac{\pi}{4} - \left[\frac{(32 + 23\lambda)\beta + 4 + \lambda}{48\beta}\right] Ca + O(Ca^2). \tag{45}$$

In weak flows free of vorticity, the stationary shape and surfactant distribution are independent of viscosity ratio since Marangoni stresses immobilize the droplet interface [77,123]. The rheological material functions for drops covered with insoluble surfactants in shear flow for surface elasticity parameter $\beta = CaMa$ are

$$\frac{\Sigma^p_{12}}{\mu\dot{\gamma}} = \frac{5}{2} - D_3(\lambda, \beta) Ca^2 + O(Ca^3), \tag{46}$$

$$\frac{N^p_1}{\mu\dot{\gamma}} = \frac{5}{2}\frac{(4\beta + 1)}{\beta} Ca, \quad \frac{N^p_2}{\mu\dot{\gamma}} = -\frac{1}{2}\frac{N^p_1}{\mu\dot{\gamma}} + \frac{75}{28} Ca, \tag{47}$$

where the coefficient D_3 is defined in Appendix A.1 Note that, in the limit of $Ca \to 0$, inserting Eq. (46) into Eq. (25) yields Einstein's classical result $1 + (5/2)\phi$ given by Eq. (27) with $g_T(\lambda) = 1$ and emulsion rheology follows the behavior of a suspension of rigid spheres with vanishing normal stress differences.

Recently, Narsimhan [60] developed a higher order small deformation theory for shape and rheology of drops covered with viscous interfaces expanding from previous classical works by Oldroyd [69] and Flumerfelt [21]. To leading order, in the limit as $\epsilon = Ca \ll 1$ and λ, Bq_s,$Bq_d \sim O(1)$

$$D_T = \frac{1}{2}\alpha_0 Ca, \quad \alpha_0 = \frac{1}{8}\frac{19\lambda + 16 + 24Bq_d + 8Bq_s}{\lambda^* + 1} \tag{48}$$

Here α_0 is the deformation parameter, $\lambda^* = \lambda + (6/5)Bq_d + (4/5)Bq_s$ is a modified viscosity ratio, and the inclination reduces to

$$\theta = \frac{\pi}{4} + \frac{Ca}{2}a_D^{-1}, \tag{49}$$

where $a_D(\lambda,\ Bq_s,\ Bq_d)$ is an expansion coefficient [60] defined in Appendix A.2. The corresponding analytical formulas for shear rheology are

$$\frac{\Sigma^p_{12}}{\mu\dot{\gamma}} = \frac{5}{2}g_T, \tag{50}$$

$$\frac{N^p_1}{\mu\dot{\gamma}} = \frac{8}{5}\alpha_0^2, \tag{51}$$

$$\frac{N^p_2}{\mu\dot{\gamma}} = -\frac{1}{2}\frac{N^p_1}{\mu\dot{\gamma}} + \frac{3\alpha_0}{70}\frac{(25\lambda^{*^2} + 41\lambda + 24Bq_d + 4)}{(\lambda^* + 1)^2}, \tag{52}$$

where shear-thinning effects are $O(Ca^2)$ contributions [60].

In the other small deformation limit when $\epsilon \ll 1$ and $Ca{=}O(1)$,

$$D_T = \frac{1}{2}\widehat{a}_E(1 + \widehat{a}_E) + O(\epsilon^3), \quad \theta = -\frac{1}{2}\frac{\widehat{a}_D}{Ca} + O(\epsilon^2), \tag{53}$$

where the small parameter $\epsilon = \lambda^{-1}$ or Bq_s^{-1} for $Bq_s \sim Bq_d$. The form of the coefficients $\widehat{a}_D$ and $\widehat{a}_E$ are shown in the Appendix A.2. In this limit, small-deformation theory indicates that the emulsions of highly viscous internal or surface viscosities behave approximately as rigid spheres with no shear-thinning and no significant elastic effects. This observation is in agreement with the small-deformation theory for high-viscosity drops in weak flows [77,78].

Droplets with slip at the interfaces Ramanchandran and Leal [59] developed a second-order small deformation analysis for drops with interfacial slip in weak flows. The model captures the anomalous decrease in relative viscosity measured in emulsions formed by immiscible polymer blends. The viscometric functions in shear flow are

$$\frac{\Sigma^p_{12}}{\mu\dot{\gamma}} = \frac{5\lambda(2\overline{\alpha} + 1) + 2}{2\lambda(5\overline{\alpha} + 1) + 2} + O(Ca^2), \tag{54}$$

$$\frac{\Sigma^p_{12}}{\mu\dot{\gamma}} = \frac{(5/2)g_T + h(\lambda, \overline{\alpha})}{1 + h(\lambda, \overline{\alpha})} + O(Ca^2), \tag{55}$$

$$\frac{N^p_1}{\mu\dot{\gamma}} = f(\lambda, \overline{\alpha})Ca, \quad \frac{N^p_2}{\mu\dot{\gamma}} = \left[\frac{g(\lambda, \overline{\alpha})}{4} - \frac{f(\lambda, \overline{\alpha})}{2}\right]Ca, \tag{56}$$

where $h(\lambda, \overline{\alpha}) = 5\lambda\overline{\alpha}/(\lambda + 1)$, and the functions f and g are defined in Appendix A.3, for completeness [59]. In uniaxial extensional flow, the theory predicts

$$\frac{\widetilde{\mu}/\mu - 3}{\phi} = \frac{5\lambda(2\overline{\alpha} + 1) + 2}{2\lambda(5\overline{\alpha} + 1) + 2} + \frac{g(\lambda, \overline{\alpha})}{4}Ca + O(Ca^2), \tag{57}$$

$$\frac{\widetilde{\mu}/\mu - 3}{\phi} = \frac{(5/2)g_T + h(\lambda, \overline{\alpha})}{1 + h(\lambda, \overline{\alpha})} + \frac{g(\lambda, \overline{\alpha})}{4}Ca + O(Ca^2), \tag{58}$$

where $\widetilde{\mu} = 3\mu$ is the Trouton viscosity for the pure suspending fluid ($\phi = 0$), and

$$\frac{\widetilde{\mu}}{\mu} = \frac{\Sigma^p_{33} - \Sigma^p_{11}}{\mu\dot{\gamma}} = \frac{\Sigma^p_{33} - \Sigma^p_{22}}{\mu\dot{\gamma}}, \tag{59}$$

by definition. The effect of interfacial slip on material functions in shear and extensional flows is more pronounced for values of viscosity ratio $\lambda > O(1)$. Slip has a stronger influence in response to extensional flows than shear flows. The analytical results indicate that slip hinders droplet deformation and decrease effective viscosity of the emulsion. However, quantitative agreement between theory and experiments is not verified even in the limit of infinite slip, suggesting that additional physical mechanisms might contribute to the pronounced viscosity reduction observed in experiments [147].

In this section on rheology of dilute emulsions, wall effects and interparticle interactions were neglected. The material functions (specific viscosity and normal stresses) for clean as well as complex interfaces show characteristics of non-Newtonian response, including a nonlinear relation between stresses and the rate of strain giving rise to fluid memory. Frankel and Acrivos [15] extended the works by Chaffey and Brenner [58], Schowalter, Chaffey and Brenner [13] and, Cox [14] to propose a set of constitutive equations that capture the transient effects of droplet deformation induced by an imposed linear time-dependent flow field. Appendix B revisits the Frankel and Acrivos analysis and retraces the steps and assumptions that lead them to a three-parameter Jeffreys-like constitutive equation for emulsions of the form

$$\Sigma_{ij} + \Lambda \frac{\mathcal{D}\Sigma_{ij}}{\mathcal{D}t} = -p\delta_{ij} + \eta\left(\dot{\gamma}_{ij} + \Lambda_J \frac{\mathcal{D}\dot{\gamma}_{ij}}{\mathcal{D}t}\right), \tag{60}$$

where we let $\dot{\gamma}_{ij} = 2E_{ij}$. The three parameters are viscosity, and two timescales. The material relaxation time is dependent on the shape relaxation time as follows:

$$\Lambda = \frac{(2\lambda+3)(19\lambda+16)}{40(\lambda+1)}\tau_\sigma = c_1(\lambda)^{-1}\tau_\sigma, \tag{61}$$

and a Jeffreys emulsion retardation time can be determined from:

$$\Lambda_J = \Lambda\left(1 - \frac{4}{5}\frac{\Lambda}{\tau_\sigma}\frac{\phi}{\eta_r(\lambda,\phi)}\right). \tag{62}$$

Nondilute emulsions: constitutive models and numerical methods

Constitutive models based on small deformation and effective medium theories

Constitutive equations proposed for nondilute emulsions aim to account for finite effects of drop deformations, interactions, and microstructure with respect to each other at dispersed-phase volume fractions typically above 10%.

Oldroyd's effective medium theory (1953) Oldroyd [12] used an effective medium approach to derive an expression for the effective viscosity of the semidilute emulsions following a perturbation analysis proposed by Frölich and Sack [70] for suspensions of elastic spheres. Finite size effects of the higher dispersed-phase volume fraction were included using a cell model. The cell model represents a composite system consisting of a drop (or a particle) surrounded by a volume of suspending fluid in a cell beyond which the emulsion (or a suspension) is seen as a continuum material. This condition is enforced by a modified far-field velocity boundary condition for the disturbance flow generated by the particle (here the generalized term particle engulfs all different types, e.g. drops, capsules, vesicles, rigid and deformable particles, and blood cells). Specifically, Eq. (4) is evaluated at a truncated far field position, $b/a \sim \phi^{-1/3}$, where b is the characteristic size of the cell in which pressure and velocity disturbances are evaluated, and a is the particle size. Oldroyd's effective medium analysis results in the following expression for the effective relative viscosity of an emulsion:

$$\eta_r = 1 + \phi\frac{5\lambda+2}{2(\lambda+1)}\left(1 + \phi\frac{(5\lambda+2)}{5(\lambda+1)}\right). \tag{63}$$

Using Taylor's factor $g_T = (\lambda + 2/5)/(\lambda + 1)$ and specific viscosity as $\eta_{sp}=(\eta_r\text{-}1)$, Oldroyd's relative viscosity relation can be rewritten in an alternative and compact form as

$$\frac{\Sigma_{12}^p}{\mu\dot{\gamma}} = \frac{\eta_{sp}}{\phi} = \frac{5}{2}g_T(1+\phi g_T). \tag{64}$$

Choi and Schowalter's small deformation theory for nondilute emulsions Choi and Schowalter [16] proposed an alternative derivation of effective viscosity of nondilute emulsions by expanding on the stress-averaged, small-deformation theories of Frankel and Acrivos [15] and Cox [14], by accounting for interparticle interactions and higher-order effects of disperse-phase volume fraction. In steady shear flow, Choi and Schowalter's constitutive equation yields the following expression for the relative viscosity of emulsions.

$$\eta_r = 1 + \phi\frac{5\lambda+2}{2(\lambda+1)}\left(1 + \phi\frac{5}{4}\frac{(5\lambda+2)}{(\lambda+1)} + O(\phi^{5/3})\right), \tag{65}$$

On comparing their expressions with Oldroyd's model from 1953, Choi and Schowalter noted that their coefficient for the second order term was 15.6 compared to 2.5 computed by Oldroyd, and the larger coefficient agrees better with the experiments and Oldroyd's expectation. Alternatively, the shear rheology response can be rewritten in terms of scaled shear stress and normal stress differences as follows:

$$\frac{\Sigma_{12}^p}{\mu\dot{\gamma}} = \frac{\eta_{sp}}{\phi} = \frac{5}{2}g_T\left(1 + \frac{25}{4}g_T\phi + O(\phi^{5/3})\right), \tag{66}$$

$$\frac{N_1^p}{\mu\dot{\gamma}} = \frac{32}{5}d_T{}^2 Ca\phi, \tag{67}$$

$$\frac{N_2^p}{N_1^p} = -\frac{1}{7}\frac{29\lambda^2+61\lambda+50}{19\lambda^2+35\lambda+16}. \tag{68}$$

the expressions for the normal stress differences, given by Eqs. (30) and (31) in Ref. [16] are presented here in alternative form. The value of N_2^p/N_1^p goes to, approximately, -0.218 for $\lambda \to \infty$ and -0.446 as $\lambda \to 0$. Furthermore, the Choi-Schowalter model leads to equations for extensional viscosity that reveal a linearly increasing value with strain rate for uniaxial and linearly decreasing value for biaxial extensional flow.

A comparison between the Choi-Schowalter model prediction based on Eq. (65) and experimental data is shown in Figure 4. The striking agreement emphasizes

Figure 4

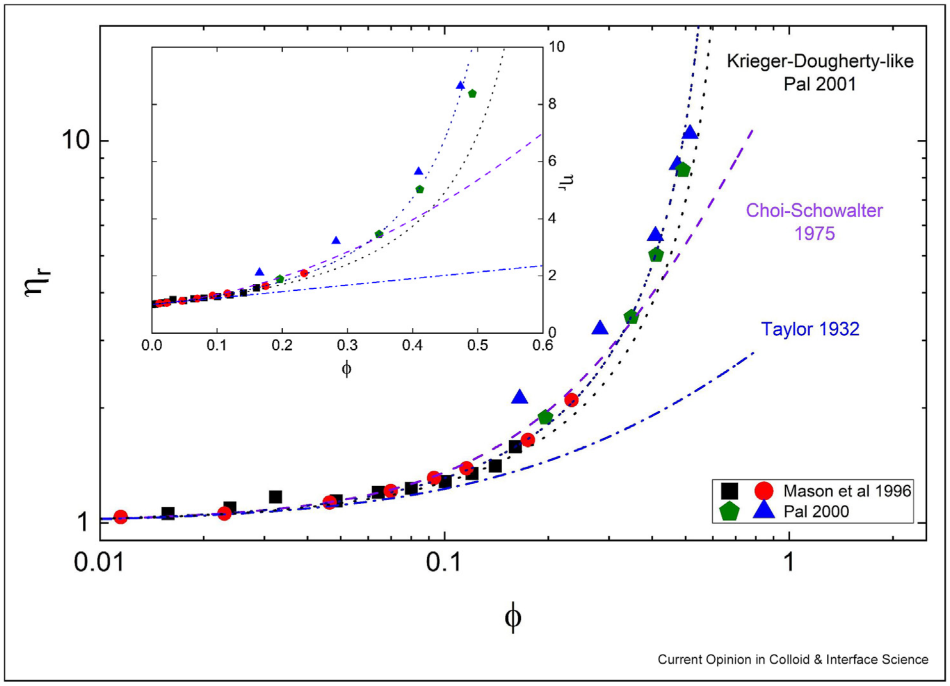

Current Opinion in Colloid & Interface Science

Comparison of theory and empirical relations for effective viscosity models of dilute and concentrated emulsions, respectively. Taylor's effective viscosity relation is obtained by inserting Eq. (39) into Eq. (25) (dash-dotted line), Choi and Schowalter is given by Eq. (65) (violet dashed line), and Eq. (70) is used for the Krieger–Dougherty-like curve (dotted lines), where two dotted lines are added: one using data from Ref. [150] (black densely dotted line), and another one with λ adjusted to best fit the experimental data (blue sparsely dotted line). See Appendix C for details on the datasets and models used.

that the model captures the observations relatively well, valid up to terms $O(\phi^2)$ in the semidilute regime. The use of logarithmic x-axis for volume fraction, ϕ helps to observe that the original analysis by Taylor [11] captures the linear dependence of η_r on ϕ in the dilute regime reasonably well. Before Choi and Schowalter [16], Yaron and Gal-Or [148] had proposed a similar model considering a free-surface cell approach, which allows for surfactant effects but without including drop deformation effects. Later generalizations of Frankel and Acrivos, Oldroyd, and Choi and Schowalter viscosity models were developed to include non-Newtonian effects of the drop and suspending phases [4,149], though a lot of open questions remain regarding the influence of viscoelasticity of the suspending or dispersed liquid phases and the interface.

Empirical equations

Empirical relations are often used to capture the effective viscosity of emulsions of spherical droplets ($Ca \to 0$) as a function of ϕ in analogy with suspensions of rigid spheres. For example, a modification of classical suspension models yields the following equation [16,72,148],

$$\eta_r = \exp\left(\frac{5/2\ \phi}{1 - \phi/\phi_m}\right)^{\alpha}, \tag{69}$$

where relative viscosity, $\eta_r \equiv \eta/\mu$ is the zero-shear-rate viscosity normalized by the viscosity of the suspending medium, and $\alpha = (2/5 + \lambda)/(1 + \lambda)$. Here ϕ_m is the emulsion maximum volume fraction at which the effective viscosity in Eq. (69) diverges. The value of ϕ_m decreases with increasing viscosity ratio ranging from 0.63 to 0.64 for high-viscosity drops [4]. In the dilute regime, $\phi \ll 1$, Eq. (69) reduces to Taylor's result (see Eq. (39)). In the limit when $\lambda \to \infty$ and arbitrary concentrations, Eq. (69) recovers a Krieger–Dougherty-like empirical viscosity relation for suspensions of hard spheres [4].

For finite values of viscosity ratio, an alternative Krieger–Dougherty-like viscosity model is [150].

$$\eta_r \left[\frac{2\eta_r + 5\lambda}{2 + 5\lambda}\right]^{3/2} = (1 - \phi/\phi_m)^{-2.5\phi_m}. \tag{70}$$

Predictions for Eq. (70) compared to experimental data are shown in Figure 4. The inset shows data plotted on a linear–linear axis. The corresponding plot shown using a log–log scale helps to emphasize how well Taylor's pioneering theory [11] captures the rheology of dilute emulsions (details about properties of dispersed and suspending liquids are included in Appendix C). The comparison of theory and experiments reveals that the Choi–Schowalter model [4,16] captures the nonlinearity introduced by drop—drop interactions in nondilute emulsions, but the impact of higher-order interactions and microstructure require a careful consideration for $\phi > 0.4$ or so. For a comprehensive review on the empirical viscosity models for concentrated emulsions see Ref. [151]. For nondilute emulsions, normal stress differences become important, and shear-thinning effects are also observed at higher shear rates [1,8,23].

Doi–Ohta, Maffettone–Minale, and other alternatives to small deformation theory

Constitutive models described so far in this article primarily focus on understanding how drop deformation influences and determines emulsion rheology, starting with Eq. (20). The small deformation theory works best for vanishingly low *Ca* values or in flows with drops closed to spherical. The results of the small deformation theories are recovered and complemented by a series of phenomenological models, inspired by the Maffettone—Minale (MM) [152], slender body or Doi-Ohta (DO) model, as briefly reviewed here. Slender body theories are used for capturing drop deformation and emulsion rheology for cases when drops are already extended to thread-like shapes, usually under high extensional flow, and though transverse cross-section is assumed to remain circular due to surface tension, the drops in the form of long fluid threads stretch and deform along their axial direction [109,141,153—155]. The alternative models are needed as emulsions formed by mechanical mixing of immiscible liquids or by phase separation can contain drops of various sizes and shapes, and during flow, these drops can deform, coalesce, and break up leading to complex evolution of drop size and shape distribution. In 1991, Doi and Ohta [156] proposed a model that characterized the emulsion rheology in terms of interfacial orientation and area, and three parameters (viscosity, surface tension, and volume fraction) but without introducing drop size as an intrinsic length scale. In 1998, Maffettone and Minale [152] provided an alternative phenomenological model for emulsion rheology by assuming ellipsoidal drops and for small to moderate deformation rates, accounted for drop rotation by vorticity, deformation by strain rate and relaxation to an unperturbed state governed by interfacial tension. Several variants of ellipsoidal models have been developed since, including for viscoelastic drops or suspending fluid, and likewise the Doi—Ohta formalism has been extended to allow for variable viscosity ratios, as summarized in several reviews [4,9,45,115,157].

The Doi—Ohta model and its descendants The Doi-Ohta model, originally proposed for equiviscous and equidense concentrated emulsions [156] adopts a coarse-grained approach to incorporate the influence of change in area and orientation of the interface to the emulsion stress. The Doi-Ohta model describes the total macroscopic stress for an emulsion as:

$$\boldsymbol{\Sigma} = \boldsymbol{\Sigma}^0 - \sigma\mathbf{q} \; = 2\mu\langle\mathbf{E}\rangle - \langle p\rangle\mathbf{I} - \sigma\mathbf{q}, \tag{71}$$

$$\mathbf{q} = \frac{1}{V}\int_S dS(\mathbf{nn} - \mathbf{I}), \quad Q = \frac{1}{V}\int_S dS. \tag{72}$$

Here, the interface tensor $\mathbf{q}$, a symmetric and second-rank tensor, tracks the orientation of the interface where dS is a differential element of interfacial area, V is the system volume, and the integral is over all interfaces. A scalar Q quantifies the amount of total interfacial area per unit volume and has dimensions of inverse length or 1/length. The interface tensor $\mathbf{q}$ and the parameter Q are related by a pair of evolution differential equations [4,156]. The original Doi—Ohta model was restricted to a concentrated emulsion, obtained from a 50-50 blend of viscosity-matched and density-matched mixture and incorporated the influence of coarsening on interfacial area and orientation on Q and $\mathbf{q}$ via scaling laws. Subsequent models retain the coarse-grained approach of the Doi—Ohta model but modify how volume fraction, formation, coalescence, and pinching of drops and coarsening are included and thereafter influence interfacial area and orientation during flow [4,9,156]. A review by Minale [9] provides a concise introduction to the different models inspired by Doi—Ohta formalism.

Ellipsoidal drops based Maffettone—Minale (MM) model and its descendants The phenomenological Maffettone and Minale model [152] assumes that drops are always ellipsoidal and incompressible (drop volume is preserved). The MM model provides the evolution equation for a symmetric, positive-definite, second-rank tensor $\mathbf{S}$ with eigenvalues representing the square semiaxes of the ellipsoid. The tensor $\mathbf{S}$ measures deviations of the droplet from the spherical shape. The nondimensional version of the equation obtained for scaled shape tensor $\overline{\mathbf{S}} = \mathbf{S}/a^2$ is as follows.

$$\begin{aligned}\frac{d\overline{\mathbf{S}}}{d\overline{t}} - Ca(\overline{\mathbf{W}}\cdot\overline{\mathbf{S}} - \overline{\mathbf{S}}\cdot\overline{\mathbf{W}}) &= -f_1{}^{MM}[\overline{\mathbf{S}} - g(\overline{\mathbf{S}})\mathbf{I}] \\ &+ f_2{}^{MM}Ca(\overline{\mathbf{E}}\cdot\overline{\mathbf{S}} + \overline{\mathbf{S}}\cdot\overline{\mathbf{E}}).\end{aligned} \tag{73}$$

The left-hand side of the MM equation involves the Jaumann derivative rotating with vorticity, and the right-hand side has the influence of interfacial tension that drives recovery to the unperturbed shape (first term) and viscous drag that deforms the drops (second term). The MM model captures experimental results for simple shear and uniaxial and planar extensional flows as long as drops remain ellipsoidal (limited in Ca range). At O(Ca), the MM model results recover Taylor's results for the following choices of the two coefficients:

$$f_1{}^{MM} = c_1(\lambda), f_2{}^{MM} = c_0(\lambda). \tag{74}$$

Minale's review [9] lists and recaps a family of models that were developed inspired by the MM model. The descendant MM models incorporate the influence of coalescence and breakup to capture the response to high deformation rates with some success, and a few variants account for cases when one of the phases is non-Newtonian [4,9,152,157]. Models from the MM family that use ellipsoid drops and allow for non-Newtonian drop or matrix phase as well as a few based on small deformation theory are able to capture the linear viscoelastic response of emulsions with reasonable success, but analysis and characterization of nonlinear viscoelasticity and response at high deformation rates remains challenging [4,9,115,149,157].

Numerical methods for concentrated emulsions

In this section, we enumerate representative numerical works on modeling semidilute to concentrated emulsion flows. We focus on the flow-induced microstructure of deformable drops in unbounded flows. Beyond the dilute regime, pairwise droplet interactions are affected by finite deformation of the drop interface allowing for hydrodynamic diffusion. Droplet deformation in the near contact is the stabilizing mechanism against coalescence in the absence of van der Waals attraction [158]. Scaling analysis for the near-contact motion between two clean drops within the lubrication regime shows slow algebraic film drainage $h/h_0 \sim \lambda/(\dot{\gamma}t)$ for $\dot{\gamma}t = O(1)$, where h is the gap between the drops and h_0 is a reference, initial gap width. At long times, the internal circulation immobilizes near-contact motion, preventing coalescence [97].

As the volume fraction of the disperse phase or ϕ increases, viscosity variation shows increasingly nonlinear increase with φ as illustrated in Figure 1, for drop-drop interactions become important, and analytical treatment is limited. In this regime, detailed numerical simulations are often used to investigate flow-induced structuring and rheology of concentrated emulsions. The choice of numerical method depends largely on the system parameters (e.g. drop relaxation time, size distribution, and dispersed-phase concentration) and imposed flow conditions. Depending on the type of problem under investigation, for example, whether changes in drop topology or the near contact approach of droplet pairs are of interest, a balance among accuracy, resolution, meshing techniques, and computational cost plays a key role in selecting the appropriate numerical method. Complex fluid flows are inherently multiphysics problems governed by phenomena across length scales (e.g. from atomistic to continuum descriptions). Continuum numerical approaches for multiphase flows are typically divided into two main categories: interface capturing and interface tracking methods [159,160].

Interface capturing and tracking methods Interface tracking methods explicitly track marker points on a grid or a mesh that fits the particle interface; classical examples are Boundary Integral Method (BIM) [161] and Immersed Boundary Method (IBM) [162]. Alternatively, interface capturing methods (e.g. Volume of Fluid Method (VoF) [163], Phase Field Method (PFM) [164], and Level Set Method (LSM) [165]) evolve a field variable across the computation domain where the interface is captured implicitly by a specific value of a field variable, for example, the contour of zeroes of the level set function [166]. At continuum scales, where volume-averaged material properties of the fluid are uniform, the interface between two immiscible fluids is often assumed to have zero thickness, hence the definition of sharp or dividing interfaces [167]. Interface tracking methods are efficient and accurate in modeling sharp interfaces and are usually the method of choice when physical parameters vary strongly across an interface. However, topological changes (e.g. coalescence and breakup) are challenging and require highly detailed meshing schemes. Interface capturing methods handle topological changes naturally, whereas interface tracking methods require additional numerical effort. For example, a numerical scheme called Arbitrary Lagrangian—Eulerian (ALE) has been proposed to track moving interfaces and resolve locally singular flows such as the pinching dynamics of fluid droplets [167]. Usually, ALE approach is combined with spatial and time discretization schemes (e.g. Galerkin Finite Element (GFEM) and Finite Differences (FDM)) and specialized meshing techniques to resolve the rapid variations of the pressure and axial velocity in the neck region during pinching [167—169]. The challenge of using interface capturing methods to model physical systems where material properties are discontinuous across an interface, may be overcome by a hybrid approach of interface-capturing methods and immersed interface methods or ghost fluid methods [114,170,171].

Particle-based models At mesoscopic length scales bridging the gap between molecular dynamics and continuum simulations, coarse-grained particle-based models (e.g. Dissipative Particle Dynamics (DPD) [172]) or kinetic-based models (e.g. Lattice Boltzmann Method (LBM) [173]) are usually employed giving access to additional physics compared to continuum-based approaches such as the BIM or LSM. However, both mesoscopic methods require large computational costs to achieve refined grid resolution typically needed in handling near-contact interactions among suspended particles accurately.

Figure 5 highlights representative numerical results of concentrated to dense emulsions using some of the methods listed in Figure 6. In a tabulated form, Figure 6 compiles a descriptive map of representative interface tracking, interface capturing, and coarse-grained mesoscopic numerical approaches used in the modeling of drop deformation in multiphase flows. The first column

Figure 5

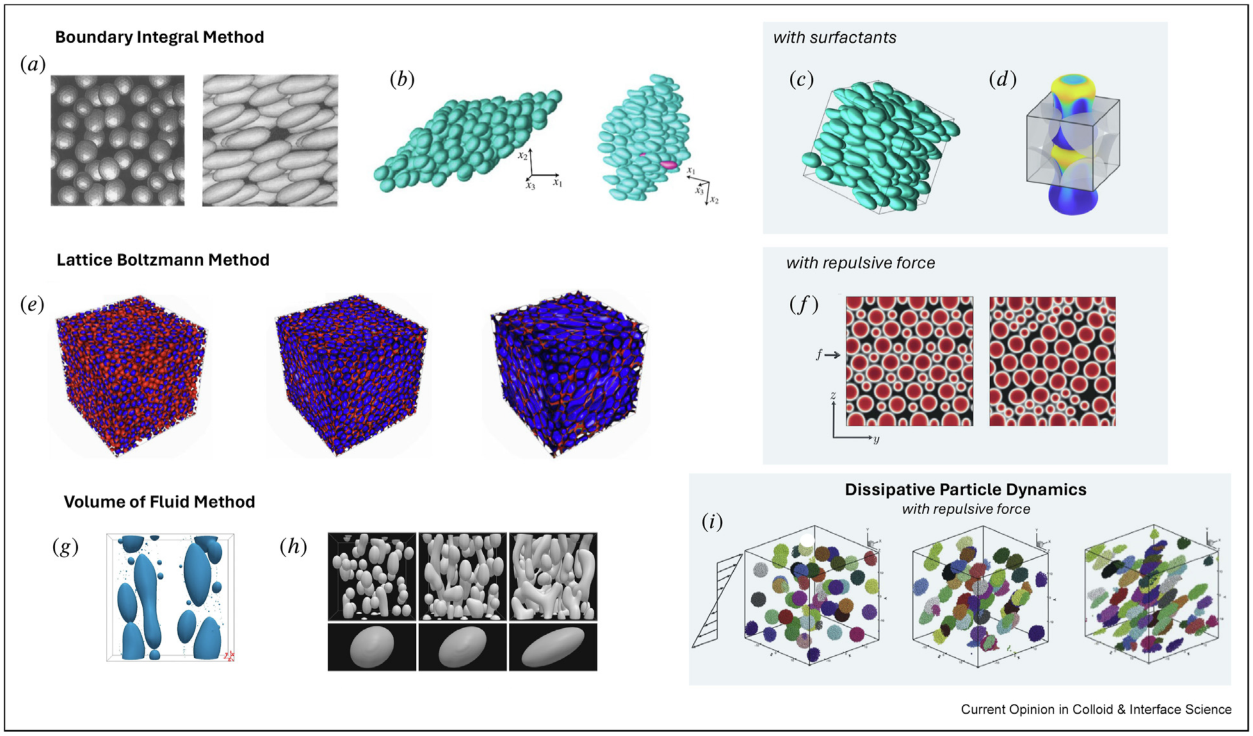

Current Opinion in Colloid & Interface Science

Summary of representative numerical works on concentrated, highly concentrated, and dense emulsions. The images are adapted from references using the Boundary Integral Method (BIM) for small-scale [174] (a) and large-scale simulations [175] (b) of clean drops in shear flow; emulsion flow of surfactant-covered droplets in shear flows [176] (c) and through structured domains [177] (d), Lattice Boltzmann Method (LBM) for flowing emulsions where stabilization against coalescence can be tuned by a repulsive force [178] (e), LBM for jammed, dense emulsions of slightly deformed droplets [179] (f), Volume of Fluid (VoF) simulations of flowing concentrated emulsions accounting for irreversible topological transitions [180] (g) and [181] (h); and Dissipative Particle Dynamics (DPD) for concentrated emulsions of droplets in shear flow [182] (i). Details of each method can be found in Fig. 6.

under each method lists the range of applicability and main features of each method, the second and third columns summarize their strengths and weaknesses, respectively. Simulating drop deformation in flowing emulsions depends highly on system parameters and on the questions under investigation. For example, if one is interested in evolving the microstructure of an emulsion at low-Reynolds number conditions where topological changes are not relevant to the system dynamics, then using BIM would be a method of choice in terms of accuracy and efficiency compared to interface capturing methods such as VoF or LSM or even coarse-grained methods like LBM. Alternatively, VoF or LSM are more efficient and stable methods compared to BIM to resolve creeping flows of concentrated emulsions where changes in topology are present since no remeshing is needed to handle coalescence or breakup events. However, handling near-contact regions between droplets hinders accuracy and increases the computational cost when using LSM and VoF. Here, our goal is to highlight that each emulsion flow problem introduces inherent physical challenges and should be probed by the appropriate numerical tool. The summary of methods listed in Figure 6 could be used as a guide.

For a comprehensive review on numerical methods used in modeling interfacial rheology, including viscoelastic effects at the interface and sharp-interface methods to solve free-surface flows, the reader is directed to Refs. [106,167], respectively, and to Ref. [160] for more details on other computational methods for multiphase flows.

Examples of numerical works on concentrated emulsions Loewenberg and Hinch [174] used boundary integral simulations and presented one of the first attempts to simulate small-scale numerical analysis of concentrated emulsion flows of clean, deformable drops with dispersed-phase volume fraction $\phi \leq 30\%$. The results showed a strong shear-thinning behavior, with large positive first and negative second normal stress differences, where typically $|N_1| > |N_2|$. This rheological response is illustrated by the microstructure anisotropy shown in Figure 5(a) where droplets are more

Figure 6

	Numerical method	Strengths	Weaknesses
(a)	**Boundary Integral Method (BIM)** - Applications: potential flow problems, electrostatics, biophysics, elasticity. - Suitable for highly viscous fluid flows. - Solves linear PDEs. - Boundary integral formulation for inviscid and Stokes flows. - Discretization of domain boundaries only.	- Reduction of dimensionality requiring fewer collocation points to solve the problem accurately. - Boundary conditions enter the formulation naturally. - Method can handle complex, deforming geometries. - Resolves near-contact drop interactions. - Highly accurate in modelling free surface flows.	- Modelling highly deformable droplets (special remeshing techniques for stability). - Elaborate mesh reconstruction techniques to capture changes in topology (not efficient). - Special analytical or numerical quadrature tools for accurate evaluation of singular integrals. - Resulting system of algebraic equations is not sparse.
(b)	**Volume of Fluid (VoF)** - Applications: fluid mechanics, heat and mass transfer, materials science, biophysics - Solves linear and non-linear PDEs. - Interface between fluids is tracked by a volume fraction field that evolves across the grid. - Finite Re number flows.	- Accurately satisfy mass conservation over time. - Tracks complex interfacial dynamics and handles topological changes. - Does not require interface reconstruction. - Built-in in most CFD software (e.g., COMSOL, Flow3D) - Straightforward implementation. - Can be combined with FEM, FD, PFM, etc.	- High computation cost to solve highly resolved domain regions (e.g., thin gap between droplets). - Higher-order interpolation schemes to resolve and maintain sharp interfaces; advected marker function is discontinuous at interfaces. - Special numerical techniques to ensure stability and accuracy for highly deformable interfaces.
	Level Set Method (LSM) - Applications: fluid mechanics, image processing, materials science, biophysics. - Solves linear and non-linear PDEs. - Geometric quantities (e.g., normal vector and mean curvature) are directly determined from the LS function. - Moving interfaces specified by the zeroes of LS function. - Finite Re number flows.	- Handles changes in topology (coalescence and breakup) naturally and efficiently. - Highly non-linear problems and shock waves can be evaluated by higher-order Up-Winding schemes. - Does not require interface reconstruction. - LSM is inherently stable and combines well with other methods (e.g., FEM, FD, PFM).	- Numerical diffusion at diffusive interface hinders accuracy of near-contact drop interactions. - Special treatment in the limit of sharp interfaces. - Periodic reinitialization is needed to enforce the LS function is a signed distance function. - High computation cost to solve highly resolved domain regions. - Mass is not conserved.
	Phase Field Method (PFM) - Applications: fluid mechanics, heat & mass transfer, materials science, biophysics. - Solves linear and non-linear PDEs. - Suitable for free-surface flows involving phase transitions (e.g., solidification). - PF variable evolves according to a Cahn-Hilliard type equation and smoothly varies between phases. - Finite Re number flows.	- Handles complex interfacial dynamics and topology. Does not require interface tracking or reconstruction. - Thermodynamically consistent formulation: variational principles of bulk and interfacial free energies. - PF can be coupled to other physical fields (e.g., temperature, stress, species concentration). - Can be combined with FEM, FD, PFM, etc.	- Numerical diffusion at diffusive interface hinders accuracy of near-contact drop interactions. - Special treatment in the limit of sharp interfaces. - Special numerical techniques to ensure stability and accuracy for highly deformable interfaces. - Enforcing boundary conditions can be challenging. - High computation cost to solve highly resolved domain regions.
(c)	**Lattice Boltzmann Method (LBM)** - Applications: fluid mechanics, heat & mass transfer materials science, biophysics. - Solves linear and non-linear PDEs. - Mesoscopic method based on kinetic theory for particle distribution functions. - Macroscopic behavior emerges from the collective behavior of fluid particles. - Fluid relaxation time is computed following collisions and induced-flux is relatable to fluid viscosity.	- Popular fluid-solver method; handles flows with complex boundary conditions. - Mesoscopic scale simulations bridging the gap between atomistic simulations and continuum approaches. - LBM can be coupled to IBM to capture fluid-structure interactions. - Discrete lattice grid: each node stores information about particle position and velocities. - Straightforward implementation, fast and parallelizable.	- Numerical diffusion and stability issues while modeling high Re number flows and flows with vanishing viscosity. - Sensitivity to model parameters (e.g., collision models and relaxation times). - Modelling fluids with non-Newtonian behavior is not trivial. - High computation cost to solve highly resolved domain regions.
	Dissipative Particle Dynamics (DPD) - Adequate to model non-equilibrium processes in complex fluids and soft matter systems (e.g., polymer physics, colloids and biological membranes) . - Coarse-grained particles and macroscopic fluid behavior emerges from the collective dynamics at particle scale. - Particle interactions are controlled by conservative, dissipative, and stochastic forces.	- Mesoscopic scale simulations bridging the gap between atomistic simulations and continuum approaches. - More efficient than atomist simulations. - Method conserves momentum which naturally recovers desirable macroscopic fluid behavior in most fluid flow applications. - Viscosity and diffusion incorporated in the formulation via dissipative and random forces.	- Coarse-grained approach does not include all molecular level physical details. - Numerical challenges in implementing complex boundary conditions and sharp variations of physical quantities across interfaces. - Sensitivity to model parameters (e.g., choice of interaction potentials).

Current Opinion in Colloid & Interface Science

Mapping of representative numerical methods typically used in simulations of concentrated emulsion flows. The three areas (a), (b), and (c) refer to interface tracking, interface capturing, and particle based methods, respectively. First column shows a general description of each method. The last two columns highlight strengths and weaknesses. Abbreviations used: Finite Element Method (FEM), Ffinite Difference (FD), Immersed Boundary Method (IBM), Computational Fluid Dynamics (CFD), partial differential equations (PDEs), Reynolds number (Re), and numerical methods as indicated.

deformed and aligned with the flow direction (left image), whereas in the vorticity direction the drops are closely packed (right image). Elongation of the droplets in the flow direction promotes large N_1 and facilitates the motion of drops past each other. This droplet arrangement reduces the collisional cross-section and local viscous dissipation, leading to a shear-thinning behavior. A similar system of interacting droplets in concentrated emulsions with $\phi < 30\%$ has been investigated, including inertial effects on the emulsion rheology and flow-induced drop structure [182]. The authors used the Dissipative Particle Dynamics method, where droplets are stabilized against coalescence by a strong repulsive force as illustrated in Figure 5(i); breakup events are not considered.

More recent studies address flow-induced structuring and rheology of highly concentrated emulsions below critical jamming conditions [175,183]. Zinchenko and Davis [183] used a large-scale boundary integral simulation to probe the rheology of highly concentrated emulsions in flows with nontrivial kinematics. Large strains were assumed, and the disperse-phase volume fraction varied in the range $0.45 < \phi < 0.55$. The simulations used 400 drops per periodic cell and improved upon earlier works from the same group [175,184]. A snapshot of a periodic cell is shown in 5(b). The authors propose a five-parameter, generalized the Oldroyd model where the variable parameters are determined from viscometric flows. For example, shear viscosity, first- and second-normal stress differences are calculated from shear flows, and extensional viscosity and stress cross-difference from extensional flows. Long-time averaged material properties in mixed shear and pure extensional flows retain the qualitative features obtained in small-scale simulations of monodisperse emulsions $\phi \leq 30\%$ [174].

Numerical analysis of drop-scale deformation and bulk rheology beyond the class of clean, deformable droplets have been mostly restricted to dilute to semidilute regimes accounting for surfactant-covered drops or drops with surface viscous dissipation [74,129,185]. Recently, Zinchenko and Davis [176] extended their numerical scheme for highly concentrated emulsion of clean drops [183] to drops covered with insoluble surfactants [176] in shear and extensional flows. They studied emulsion flows with dispersed-phase volume fractions $0.45 < \phi < 0.6$, viscosity ratio $0.25 < \lambda < 3$, and surfactant elasticity $0.05 < \beta < 0.2$. Sophisticated meshing schemes needed to capture highly deformed droplets in nearly jammed dense emulsions and numerical resolution of the near-contact phenomena of approaching droplets are challenges faced by researchers in this field. A representative snapshot of a highly-concentration emulsion of surfactant-covered droplets in shear flow is shown in Figure 5(c). Figure 5(d) shows BIM simulations of a pair of highly deformable surfactant-covered droplets flowing through a pore geometry; the color gradient along the surface indicates regions of different surfactant concentration.

Influence of drop coalescence and breakup Transient evolution of the emulsion microstructure in concentrated emulsions, including changes in droplet topology (e.g. breakup and coalescence events) remains an open area of research. The critical effect of flow-induced droplet breakup and fragmentation on the microstructure and rheology of emulsions [135,186], including wall effects [45,82,83,85,87,187], external force fields [81,86,188], non-Newtonian contributions from either the dispersed or continuous phases (e.g. viscoelastic, power-law, elastoviscoplastic) have been reviewed or studied elsewhere [45,188–191].

Coalescence and breakup events may coexist in confined emulsion flows, leading to nontrivial rheology. For example, shear bands, which are regions of high and low droplet concentrations in the vorticity and flow direction, respectively, have been observed in numerical experiments [180,192]. Figure 5(g) shows a snapshot of the droplet microstructure in VoF simulations adapted from Ref. [180]. Rosti et al. [181] determined the effective viscosity of concentrated emulsions using a 3-dimensional VoF method for volume fractions in the range $10^{-3} < \phi < 0.3$ and capillary number $0.1 < Ca < 0.3$. Coalescence events lead to a nonmonotonic variation of effective viscosity with ϕ, with a peak around $\phi \approx 0.20$. The representative droplet shape distribution observed in their VoF simulation is shown in Figure 5(h). Recently, Girotto et al. [178] used the mesoscopic LBM to study the evolution of the microstructure of emulsions as the disperse-phase volume fraction increases from semi-dilute to jammed configurations. The authors included coalescence and breakup events and further studied aging dynamics effects after the flow is stopped. An evolution of the emulsion droplet network as the concentration increases is shown in Figure 5(e). For a comprehensive review on numerical aspects and recent progress on the modeling of deformable particles in flows using the LBM see Ref. [193]. Peterson et al. [194] proposed a generalized framework model for droplet breakup in dense emulsion flows using a population balance model coupled to droplet shape evolution.

Jammed dense emulsions with polygonal drops in a network of films

On increasing the volume of the dispersed phase or ϕ beyond the highly concentrated regime of flowing emulsions discussed in the previous section, the rheological response shows the manifestation of a yield stress, implying flow occurs only after a minimum threshold value of stress (or applied force) is exceeded. The magnitude of yield stress and the flow behavior displayed for $\tau > \tau_Y$ show a high sensitivity to the positional structure, size, shape, interparticle forces, and polydispersity of droplets. In this regime, an emulsion of repulsive droplets (stabilized against coalescence) transitions from amorphous, glass-like behavior for $\phi_g \approx 0.58$ to a jammed, dense regime at $\phi \approx \phi_{RCP}$, where the microstructure is dense and randomly packed and $\phi_{RCP} \approx 0.64$. In the limit as $\phi \rightarrow 1$, the drops get compressed into polygonal shapes. The deformed drops are separated by thin films of the continuous phase fluid, and the films that intersect at Plateau borders thus develop a microstructure or a castle of polyhedral shapes characteristic of dry foams [1,4,8,23,43,195]. In this section, we focus on the structure and rheology of jammed dense emulsions where the droplets are densely packed, showing a solid-like behavior under weak loading and a fluid-like behavior beyond an effective yield stress [41,196].

Dilute and nondilute flowing emulsions, as discussed in sections 4-5, exhibit a non-Newtonian rheology and viscoelastic response, and their elasticity is attributed at the drop level to the interfacial tension-dependent shape relaxation time. Jammed dense emulsions show a viscoplastic response to imposed bulk stresses, such that flow only occurs after yield stress is exceeded. The empirical Herschel—Bulkley (HB) model is often used for capturing the flow behavior for a complex fluid that displays a yield stress and flows with a power law relationship between stress and deformation rate above yield stress. The three-parameter HB model includes a power law exponent, n, consistency, K, and yield stress, τ_Y, and can be written as

$$\tau = \tau_Y + K\dot{\gamma}^n = \tau_Y + \tau_v(\dot{\gamma}). \qquad (75)$$

The HB model is a generalization of the Bingham model that includes only two parameters (as the power law exponent equals 1). More elaborate models such as soft glassy rheology (SGR) model, mode coupling theory can be derived to capture the rheological behavior of yield stress materials by accounting for local traps or local rearrangement zones in dispersions containing densely packed drops or particles, as detailed elsewhere [4,197,198].

The viscoplastic behavior may be qualitatively defined using the Bingham number, Bn

$$Bn = \frac{\tau_Y}{\tau_c}, \qquad (76)$$

which is simply the ratio of yield stress τ_Y and an imposed characteristic stress, $\tau_c = \mu U/L$. Here μ is characteristic viscosity, U and L are characteristic velocity and length scale, respectively.

Under small strains, and small stresses compared to τ_Y, dense emulsions show a jammed, solid-like behavior with elastic modulus given by

$$G \approx \frac{\sigma}{a_{32}}\phi^{1/3}(\phi - \phi_0), \qquad (77)$$

where σ is the interfacial tension coefficient, $a_{32} = 3$ V/A is a volume-to-surface-area mean drop radius, and $\phi_0 \approx 0.71$ is the limiting volume fraction at which the percolation of the droplet network collapses. The rheology of dense emulsions of noncoalescing droplets, including typical flow curves and characteristic viscoelastic behavior described by the storage, G', and loss moduli, G'', subject to linear and nonlinear viscoelastic flowing regimes and has been well documented in reviews and papers [1,8,23,56,187,195], where most of the works are experimental. Theory and numerical aspects of the problem remain an active area of research.

The measurement or observation of an apparent yield stress in jammed dense emulsions and suspension of particles with a relatively wide range of interaction is much easier than describing the underlying mechanism involving the dynamics of dispersed drops in the case of emulsions [7,57,197,199—202]. The collapse of the amorphous, glass-like microstructure signals the transition to a fluid-like behavior where a classical empirical model by Princen and Kiss [41] for the yield stress is

$$\tau_Y = \frac{\sigma}{a_{32}}\phi^{1/3}Y(\phi), \qquad (78)$$

and $Y(\phi)$ is an empirical relation showing a logarithmic dependence on ϕ [41]. Several models are proposed as detailed in the review by Kim and Mason [8]. Figure 6 illustrates that two empirical models capture the trends observed experimentally for ϕ dependent increase in modulus and yield stress. Details including the properties of dispersed and suspending fluid, the expression for computing the two quantities, and values used for different constants are listed in the Appendix for completeness. For emulsions that display yield stress, recent experiments using gravity-based rheometry show the possibility of measuring both an extensional yield stress and the power law relation between extensional stress and strain rate using analysis of dripping, though challenges remain in quantitatively describing the underlying mechanisms for strong flows where droplet deformability probably plays a role [26,28,89,200].

Denkov and coworkers [206] argued that the second term or the viscous stress contribution, $\tau_v(\dot{\gamma})$ for yielded emulsions can be attributed to the energy dissipation in thin films between neighboring drops sliding along each other. Their model anticipates a power law exponent $n = 1/2$ if disjoining pressure is neglected and explains why viscous stress and shear viscosity exhibit $Ca^{1/2}$ and $Ca^{-1/2}$ scaling, respectively, for flowing emulsions. An extended version of the model suggests $n < 1/2$ if interfacial dissipation plays a role and $n > 1/2$ if disjoining pressure exerts an influence. The model appears to capture the diversity in power law exponents observed experimentally in flowing emulsions [206,207].

Numerical studies of jammed dense emulsions Emulsions display ϕ dependent yield stress and is often used by experimentalists as a model system for investigating rheological response. Numerically modeling jammed dense emulsions proffers a similar opportunity with the advantage that changes in microstructure below and above yield stress in response to applied stress can be visualized and analyzed, as shown in a recent numerical investigation by Negro et al. [179]. The authors numerically investigated in 2D the yield stress and flow behavior of a model emulsion that contains an amorphous, deformable, non-coalescing droplets embedded in a Newtonian fluid, as summarized below.

Negro et al. [179] evolved the droplet dynamics using the 2D hybrid LBM and computed hydrodynamics by following the evolution of phase field variables and velocity of the suspending fluid using the Cahn–Hilliard equation. The droplets are stabilized against coalescence by a soft repulsion force providing for a weak overlap between droplets and forming a percolated microstructure. The model system of densely packed droplets of conserved area initially lies in an amorphous, immobile, glass-like state in response to an external forcing, f or pressure difference in a parabolic flow. When the forcing is greater than a critical value f_c, the percolated network yields, and the microstructure orders along the flow direction. Even for $f < f_c$, numerical results indicate the continuous fluid permeates the immobile droplet network and hence the effective viscosity is large but finite. Yielding transition is marked by droplet mean velocity fluctuations and stick-slip fluid motion. An analysis of bidisperse systems of small and large species reveals a similar phase transition occurs for $f > f_c$. In this regime, yielding is followed by an ordered microstructure where large species accumulated near the centerline of the pressure-driven flow and small species are marginated, as shown in Figure 5(f). This behavior is reminiscent of flow-induced structuring in the bulk and near the boundaries of dilute to concentrated suspensions given by a balance among

Figure 7

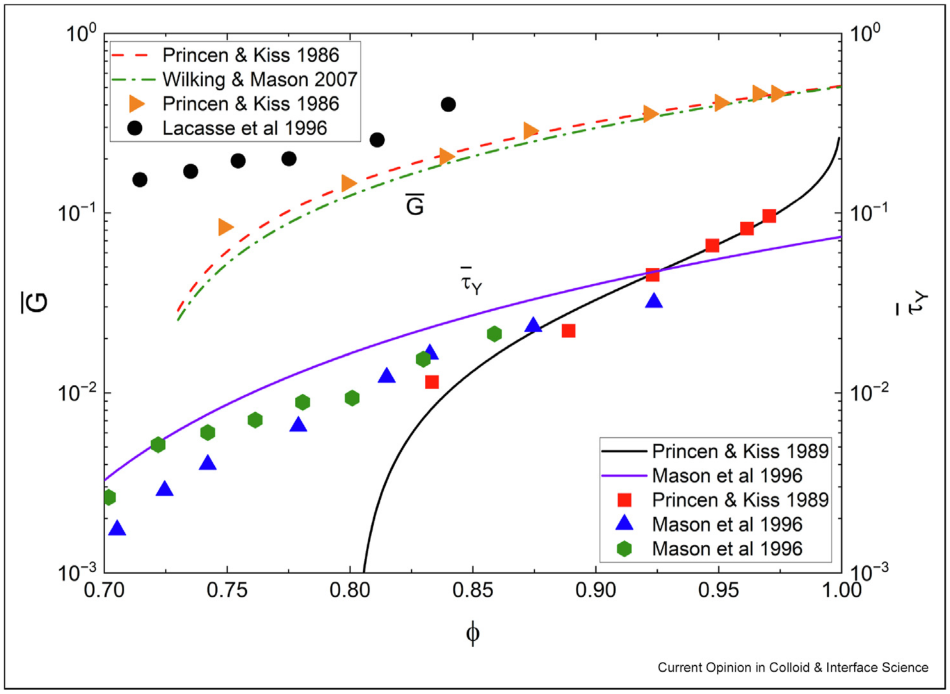

Comparison between elastic modulus and yield stress empirical models for jammed dense emulsions. Data sets obtained from Refs. [203,204] for elastic modulus and from Refs. [41,42] for yield stress. Empirical models for elastic modulus obtained from Refs. [203,205], and for yield stress from Refs. [41,42]. Both elastic modulus and yield stress are normalized by a characteristic capillary stress σ/a. See Appendix C for details on the datasets and models used.

Figure 8

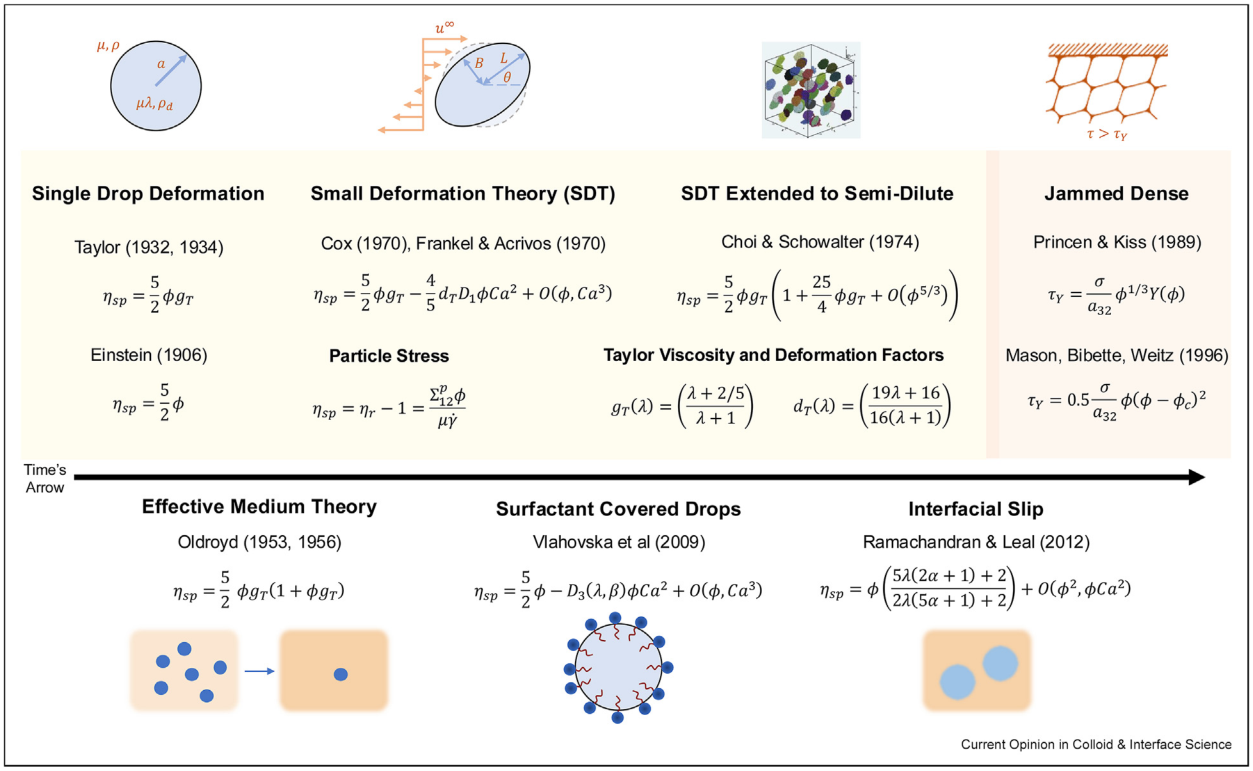

Current Opinion in Colloid & Interface Science

A compendium of analytical expressions for relative viscosity for dilute to nondilute emulsions derived using small deformation or effective medium theory and phenomenological relations for yield stress in jammed dense emulsions. The publication years are included for each model to highlight the milestones corresponding to time's arrow.

hydrodynamic diffusion, deformation-induced drift velocity, and local velocity gradient fluxes [158,208–217].

Challenges, opportunities, and prognosis

Over the past century, the progress in describing the physicochemical origins of the flow behavior of emulsions reflects progress in describing soft matter physics, thermodynamics, intermolecular and surface forces, interfacial properties, and drop deformation, breakup and coalescence. Despite progress, designing more sustainable, cost-efficient, or functional emulsion-based formulations remains challenging as many fundamental scientific problems arise. The macromolecular, supramolecular and particulate ingredients can alter the rheology of dispersed or suspending fluids and influence interfacial properties, affecting the stability, application, and processing of emulsions. The review captures some highlights from the current state-of-the-art in modeling shear rheology of emulsions containing Newtonian drops in Newtonian continuum phase with a Newtonian interface. Making any of the three non-Newtonian introduces conceptual, characterization, and modeling challenges. Additional open questions are encountered in the following contexts, where we restrict discussion to theoretical and computational challenges only.

Extensional rheology response requires a careful consideration of large changes in drop shapes, which enhances the possibility of breakup or coalescence of drops and microstructure changes, which in turn influences the response of streamwise velocity gradients [218]. For nondilute emulsions, there is also a pronounced lack of experimental data that can be used to benchmark theoretical methods. There is a lack of in-situ techniques that can be used to measure extensional viscosity while visualizing the evolution of drop shapes and microstructure in response to practically relevant deformation rates [26–28].

Influence of non-Newtonian interfacial rheology Connecting the emulsion rheology response to the specific measures of interfacial rheology response in dilatational, shear, elastic, bending, and torsion modes remains a challenge that can benefit from a combination of modeling and experimental studies [19]. Adsorbed layers of proteins, surfactants, polymers, particles, and lipids can display interfacial properties ranging from mobile to rigid, spanning theories discussed herein to describing drops with clean interfaces to elastic interfaces (like capsules) [1,18–20,60,67,68].

Viscoelastic dispersed or suspending fluid Despite significant progress in analyzing drop deformation for cases with either phase or both phases are non-Newtonian, the constitutive models and numerical studies described in this contribution are inadequate for capturing the rheological response at high deformation rates for emulsions containing viscoelastic suspending fluids or viscoelastic droplets in a Newtonian suspending medium. The two-way coupling of bulk elastic stresses to the interfacial stress jump across the interface can be highly nonlinear, introducing challenges in modeling multiphase flows containing moving boundaries. The effect of flow-induced cross-stream migration and deformation of droplets or capsules in viscoelastic background fluids on the rheology of dilute to concentrated suspensions also remains an open area of research [1,45,219,220].

Bubbly fluids Theoretical and experimental investigations on the transient rheology of bubble suspensions remain an active area of research [221,222]. In the limit of emulsions containing bubbles as the dispersed phase ($\lambda \rightarrow 0$), Rust and Manga [223,224] compared small and large deformation theories and numerical calculations to experimental results on the shape, deformation, and effective viscosity of surfactant-free bubbly suspensions. Around the same time, Llewellin et al. [225] proposed a constitutive model to study the transient rheology of polydisperse bubble suspensions derived using the small deformation theory of Frankel and Acrivos [15] that reduces to a three-parameter Jeffrey-like model typically used to characterize the rheological response of viscoelastic liquids, as shown in Eq. (60) [10].

Role of deformation and processing history, including emulsification Changes in drop sizes and size distributions and microstructure have a direct impact on the overall flow properties of emulsions. Modeling different emulsification methods [33,34,103,104,154] and polydisperse droplets to emulate the formulations used in personal care, food, or industry-grade emulsions requires a deeper dive into the rheology and thermodynamics of multicomponent systems [1–3,18,46,49,91,226].

Yielding and microstructural evolution of jammed dense emulsions Further research is needed to elucidate the effects of changes in local drop size, shape and number density, and topological changes involving interconnected thin films on the bulk rheology of emulsions, especially if disjoining pressure and interfacial rheology effects are to be included, and if non-Newtonian phases are involved [4,8,28,43,57,89,96,197,200].

We close this overview with Figure 8 which highlights the key equations and the underlying physicochemical considerations described in this contribution. Figure 8 includes a timeline of analytical relative viscosity models from dilute to semi-dilute systems and phenomenological relations for yield stress of jammed dense emulsions. We offer this survey of theoretical and numerical modeling of emulsions rheology to the scientific community, with the awareness that despite this remarkable progress, many practical problems remain in producing, storing, processing, and designing emulsions. We anticipate that advances in numerical and computational methods and the emergence of exciting problems and consumer/industry-driven quests involving food and personal care emulsions made with sustainable ingredients will drive the field in the near future.

Declaration of competing interest

The authors declare that they have no known competing financial interests or personal relationships that could have appeared to influence the work reported in this paper.

Acknowledgements

For discussions on the key aspects of fundamental and applied emulsion rheology and feedback on early draft versions, the authors wish to acknowledge Stefan Baier, Hy Bui, Philip Erni, Peter Fischer, Marc-Antoine Fardin, Reza Foudazi, Shamsheer Mahammad, Vivek Narsimhan, Taygoara Oliveira, Joe Peterson, Arun Ramachandran, Naveen Reddy, Abhinendra Singh, Samanvaya Srivastava and Siva Vanapalli. We wish to dedicate the review to Andreas Acrivos for Vivek's interactions with Andy during his sabbatical stint at the Stanford University in Fall 2022 motivated an initial dive through many fundamental papers included here. Rodrigo acknowledges the Department of Chemical Engineering and the Office of Diversity, Equity & Engagement at UIC for funding and research support as a Bridge to Faculty Postdoctoral Fellow. Nadia acknowledges the Department of Chemical Engineering at UIC for teaching assistantship and the Kraft Heinz Company for funding.

Appendix.

A. Small deformation theory: clean drops distortion tensor.

In the limit when suspended neutrally buoyant, the clean droplet deviates from sphericity only slightly; the droplet surface is given by Ref. [88].

$$S(t) = r(t) - a\left(1 + \epsilon\frac{\mathbf{x}\cdot\mathbf{A}(t)\cdot\mathbf{x}}{r^2}\right) + O(\epsilon^2) = 0 \qquad (79)$$

where $\epsilon \ll 1$ is a small parameter, $\mathbf{A}$ is the shape distortion tensor, a is the radius of the undeformed, spherical droplet, and $r = (\mathbf{x}\cdot\mathbf{x})^{1/2}$ is the radial position measured from the droplet center. The shape distortion tensor is a measure of elongations of material lines of a deformable body,

$$\frac{ds}{ds_0} = \left(1 - 2\epsilon\frac{\mathbf{x}}{r}\cdot\mathbf{A}\cdot\frac{\mathbf{x}}{r}\right)^{-1/2}, \qquad (80)$$

where ds_0 and ds are the lengths of a material line at a reference and current configuration. By definition, the shape distortion tensor $\mathbf{A} = \left(\mathbf{I} - \mathbf{B}^{-1}\right)/2$, where $\mathbf{B}=\mathbf{F}\cdot\mathbf{F}^T$ is the left Cauchy–Green deformation tensor and $\mathbf{F}$ is the deformation gradient tensor. The deformation gradient tensor is a second order tensor that maps the deformation of material lines from a reference to a current configuration $d\mathbf{x} = \mathbf{F}\cdot d\mathbf{x}_0$ whose components are $F_{ij} = \partial x_i/\partial x_{0j}$ [145]. Taking a Taylor series expansion of the right-hand-side of Eq. (80) yields,

$$\frac{ds}{ds_0} = 1 + \epsilon\frac{\mathbf{x}}{r}\cdot\mathbf{A}\cdot\frac{\mathbf{x}}{r} + \epsilon^2\frac{3}{2}\frac{\mathbf{xx}:\mathbf{AA}:\mathbf{xx}}{r^4} + \ldots. \qquad (81)$$

Equation (79) is obtained from relation (81), noting that perturbations in the droplet shape are captured by $r(t) = a(ds/ds_0)$, and hence the surface is defined by $S(t) = r(t) - ds/ds_0 \equiv 0$ to leading order in ϵ.

The solutions to Eqs. (2) and (3) are obtained assuming a spherical shape by, for example, superposition of vector spherical harmonics [102]. To leading order, shape distortions are captured in the definition of the normal vector $\mathbf{n} = \nabla S(t)/|\nabla S(t)|$ such that [78].

$$\mathbf{n} = \frac{\mathbf{x}}{r} - 2a\,\epsilon\left[\frac{\mathbf{A}\cdot\mathbf{x}}{r^2} - \frac{\mathbf{x}(\mathbf{x}\cdot\mathbf{A}\cdot\mathbf{x})}{r^4} + O(\epsilon^2)\right], \qquad (82)$$

and hence appears in the calculation of the mean curvature, H, given by Eq. (7). Enforcing boundary conditions (5) and (6) at the droplet interface, the leading order interfacial velocity reduces to

$$\mathbf{u}_s = \mathbf{W}\cdot\mathbf{x} + c_0(\lambda)\mathbf{E}\cdot\mathbf{x} - \frac{\sigma}{\mu a}c_1(\lambda)\,\epsilon\mathbf{A}\cdot\mathbf{x}, \qquad (83)$$

where $c_0(\lambda) = 5/(2\lambda+3)$, $c_1(\lambda) = 40(\lambda+1)/[(19\lambda+16)(2\lambda+3)]$, and $\mathbf{E}$ and $\mathbf{W}$ are the imposed-flow rate-of-strain and vorticity tensors, respectively, i.e. $\mathbf{u}^\infty = (\mathbf{E}+\mathbf{W})\cdot\mathbf{x}$. Inserting Eq. (33) into the kinematic boundary condition (10) written in the form $DS(t)/Dt = 0$, where $D/Dt = \partial/\partial t + \mathbf{u}\cdot\nabla$ is the material derivative [117], and using the approximation that $D(\mathbf{x}/r)/Dt \approx \mathbf{W}\cdot\mathbf{x}/r$, $Dr/Dt = (\mathbf{x}/r)\cdot\mathbf{u}_s$, and that $\mathbf{W}$ is antisymmetric yields the evolution equation for the distortion tensor [32,78].

A.1 Second-order deformation theory coefficients: clean droplets

For completeness, the coefficients appearing in Eqs. 39)-(24 for clean drops are listed below [77],

$$D_0(\lambda) = \frac{(19\chi - 3)}{20\chi} = \frac{(19\lambda + 16)}{20(\lambda + 1)} = \frac{4}{5}d_T, \qquad (84)$$

and

$$D_1(\lambda) = \left(-3888 - 27308\chi + 231041\chi^2 - 33637\chi^3 - 189761\chi^4 + 159201\chi^5\right)/(35280\chi^4), \qquad (85)$$

and in Eq. (41), the second-order deformation analysis for clean drops includes

$$D_2(\lambda) = \frac{3[12 + 9(1+\lambda) - 25(1+\lambda)^2]}{28(1+\lambda)^2} \qquad (86)$$

Likewise in Eq. (46) for droplets covered with insoluble surfactants [77],

$$D_3 = \frac{5}{1176\beta^2}[245\chi + 98\beta(3+\chi) + \beta^2(-1059 + 1127\chi)], \qquad (87)$$

where $\chi = 1 + \lambda$ and $\beta = CaMa$.

A.2 Droplets with viscous interface

Coefficients needed in the analytical formulas for droplets covered with viscous interfaces are listed in this appendix, for completeness. A full analysis for small deformation analytical results in shear and extensional flows are listed in Ref. [60]. The coefficient in inclination angle formula Eq. (49) in the limit when the small parameter $\epsilon = Ca$ is

$$a_D = [-8(6Bq_d + 4Bq_s + 5\lambda + 5)]/(64Bq_d + 48Bq_s + 89\lambda + 46Bq_d\lambda + 52Bq_s\lambda + 38\lambda^2 + 32Bq_dBq_s + 48). \qquad (88)$$

The coefficients appearing in Eq. (48) in the limit when $\epsilon = \lambda^{-1}$ and $Bq_s \sim Bq_s = O(1)$,

$$\widehat{a}_D = -\frac{20}{19}\epsilon, \qquad (89)$$

$$\widehat{a}_E = \frac{5}{2}\epsilon - \epsilon^2\left(\frac{15}{4}+\frac{5}{38}Bq_d+\frac{45}{19}q_s\right), \tag{90}$$

and when $\lambda = O(1)$ and $\epsilon = Bq_i^{-1}$ where $i = s$, d and $Bq_s \sim Bq_d$ are

$$\widehat{a}_D = -\epsilon\left(\frac{3}{2}+\frac{Bq_s}{Bq_d}\right), \tag{91}$$

$$\begin{aligned}\widehat{a}_E &= \frac{5}{4}\epsilon\left(3+\frac{Bq_s}{Bq_d}\right) - \frac{5}{64}\epsilon^2\Big[96+69\lambda+(72+63\lambda)\\ &\quad\times(Bq_s/Bq_d)+(24+26\lambda)(Bq_s/Bq_d)^2\Big].\end{aligned} \tag{92}$$

A.3 Droplets with interfacial slip

The coefficients appearing in Eqs. (54)–(56) for the viscometric functions of droplets with slip in shear flow are [59]

$$f = \frac{1}{40}\left[\frac{\lambda(80\overline{\alpha}+19)+16}{\lambda(5\overline{\alpha}+1)+1}\right]^2, \tag{93}$$

and

$$\begin{aligned}g &= \left(3[\lambda(80\overline{\alpha}+19)+16]\left[5\lambda^2(20\overline{\alpha}^2+4\overline{\alpha}+5)+4\right.\right.\\ &\quad\left.\left.+\lambda(40\overline{\alpha}+41)\right]\right)\Big/\left(140[\lambda(5\overline{\alpha}+1)+1]^3\right),\end{aligned} \tag{94}$$

where $\overline{\alpha}$ is the dimensionless slip coefficient defined in Constitutive models for dilute emulsions.

B. Constitutive equation for dilute emulsion of clean droplets

In this Appendix we present a discussion and list the main equations for a constitutive equation for a dilute emulsion of nearly spherical, clean drops with finite surface tension following the work by Frankel and Acrivos [15]. Under small deformation conditions, the particle extra stress contribution as shown in Eq. (21) reduces to

$$\begin{aligned}\Sigma^p_{ij} &= \mu_0\phi\left\{\frac{10(\lambda-1)}{2\lambda+3}E_{ij} - \frac{24}{2\lambda+3}F_{ij}\right.\\ &\quad+\frac{360(\lambda-1)^2}{7(2\lambda+3)^2}\tau_\sigma\mathcal{L}[F_{ip}E_{pj}]\\ &\quad\left.+\frac{288(\lambda-6)}{7(2\lambda+3)^2}\tau_\sigma\mathcal{L}[F_{ip}F_{pj}]+O(\dot{\gamma}Ca^2)\right\},\end{aligned} \tag{95}$$

when $\epsilon = Ca$ and λ is arbitrary, where $\tau_\sigma = \mu a/\sigma$ is the material relaxation time, F_{ij} are the components of a second-order tensor that defines a shape distorting parameter f, such that, to leading order according to Eq. (33),

$$f = F_{ij}\left(\frac{\partial^2 r^{-1}}{\partial x_i \partial x_j}\right)_{r=a} = \frac{\mathbf{x}\cdot\mathbf{A}\cdot\mathbf{x}}{r^2}. \tag{96}$$

The coefficient of the shape distorting parameter satisfies an evolution equation,

$$\begin{aligned}F_{ij}+g_1(\lambda)\tau_\sigma\frac{\mathcal{D}F_{ij}}{\mathcal{D}t} &= g_2(\lambda)E_{ij}+g_3(\lambda)\tau_\sigma\mathcal{L}[F_{ip}E_{pj}]\\ &\quad+g_4(\lambda)\tau_\sigma\mathcal{L}[F_{ip}F_{pj}]+O(\dot{\gamma}Ca^2),\end{aligned} \tag{97}$$

where

$$\mathcal{L}M_{ij} = \frac{1}{2}\left(M_{ij}+M_{ji}\right) - \delta_{ij}M_{ll}, \tag{98}$$

is a linear operator that yields the symmetric, traceless part of a second order tensor $\mathbf{M}$, δ_{ij} is the Kronecker delta, and the operator $\mathcal{D}/\mathcal{D}t$ is the co-rotational, Jaumann derivative that translates and rotates with the particle [227],

$$\frac{\mathcal{D}M_{ij}}{\mathcal{D}t} = \frac{\partial M_{ij}}{\partial t}+u_k\frac{\partial M_{ij}}{\partial x_k}+W_{ik}M_{kj}-W_{kj}M_{ik} \tag{99}$$

where $\mathbf{W}$ is the vorticity tensor. The functions appearing in Eq. (97) are listed in the Appendix. In the limit when $\epsilon = \lambda^{-1} \ll 1$ for arbitrary, finite Ca, Eqs. (95) and (97) reduced to

$$\begin{aligned}\Sigma^p_{ij} &= \mu_0\phi\Big\{5E_{ij}+12(\tau_\sigma\lambda)^{-1}F_{ij}\\ &\quad+\frac{90}{7}\lambda^{-1}\mathcal{L}[F_{ip}E_{pj}]+O(\dot{\gamma}\lambda^{-2})\Big\},\end{aligned} \tag{100}$$

and

$$\begin{aligned}&\frac{20}{19}(\tau_\sigma\lambda)^{-1}F_{ij}+\frac{\mathcal{D}F_{ij}}{\mathcal{D}t} =\\ &(5/6)E_{ij}-(10/7)\lambda^{-1}\mathcal{L}[F_{ip}E_{pj}]+O(\dot{\gamma}\lambda^{-2}).\end{aligned} \tag{101}$$

The constitutive equations (21), (95) and (100) are the main results of Frankel and Acrivos small deformation theory for an emulsion of clean droplets. These results are in agreement with constitutive equations derived for suspensions of solid elastic [228] and for emulsions with an intrinsic material relaxation time [229].

For steady or weakly time-dependent flows, in the limit when $\epsilon = Ca \ll 1$ and $\tau_\sigma|\mathbf{E}\cdot\mathbf{E}|\ll|\mathbf{E}|$, Eq. (95) can be recast in the form of Oldroyd's constitutive equation [229],

$$\Sigma_{ij} + \Lambda\frac{\mathcal{D}\Sigma_{ij}}{\mathcal{D}t} = -p\delta_{ij} + 2\mu\eta_r\left(E_{ij} + \Lambda\frac{\mathcal{D}E_{ij}}{\mathcal{D}t}\right) + \Lambda\mu\phi\Bigg\{-\frac{8}{5}\left(\frac{\Lambda}{\tau_\sigma}\right)\frac{\mathcal{D}E_{ij}}{\mathcal{D}t} + \frac{1}{(2\lambda+3)}\left[\frac{150}{7}g_T^2(\lambda) + 18\frac{\lambda}{(\lambda+1)^2}\right]\mathcal{L}\left[E_{ip}E_{pj}\right]\Bigg\} \tag{102}$$

where η_r is the emulsion relative viscosity, $\mathcal{L}$ is a symmetric, traceless operator given by Eq. (98), $\mathcal{D}/\mathcal{D}t$ is the Jaumann derivative defined in Eq. (99), Σ_{ij} are the components of the volume-averaged stress tensor defined in Eq. (21), and the timescale computed using

$$\Lambda = \frac{(2\lambda+3)(19\lambda+16)}{40(\lambda+1)}\tau_\sigma = c_1(\lambda)^{-1}\tau_\sigma, \tag{103}$$

represents a material relaxation time due to finite values of surface tension, which recovers the shape relaxation time defined in Eq. (34) in terms of the coefficient $c_1(\lambda)$ multiplying the distortion tensor $\mathbf{A}$. Following Oldroyd's findings [229], Eq. (102) describes a viscoelastic fluid with non-zero normal stress differences, a shear-rate dependent relative viscosity, and a positive Weissenberg effect [15]. These results are confirmed by second-order small deformation theory given by Eqs. (39)−(41).

Fundamental aspects of rheological constitutive equations of state, such as invariance properties, have been discussed in a classical work by Oldroyd [230] for dilute emulsions. At sufficiently weak flows with small enough velocity gradients, the last term in Eq. (102) has a higher-order contribution to the total particle stress and Eq. (102) reduces to a three-parameter, Jeffrey-like constitutive equation given by Eq. (60) in the main text.

C. Data used in Figures 3 , 4 and 7

C.1 Experimental datasets used in Figure 3

The schematics redrawn and used in Figure 3 are adapted from the experimental results detailed in Ref. [136].

- First row: $\lambda = 6$. Silicone oil 30,000 (Dow Corning fluid) in 60 cP oxidized castor oil (Pale 4). Interfacial tension 6.0 dyn/cm.
- Second row: $\lambda = 1$. Oxidized castor oil (Pale 4) in 52.6 cP silicone oil 5000 (Dow Corning fluid). Interfacial tension 4.8 dyn/cm.
- Third row: $\lambda = 0.7$. Oxidized castor oil (Pale 4) in 90 cP corn syrup. Interfacial tension 21 dyn/cm.
- Fourth row: $\lambda = 0.0002$. Distilled water in 52.6 cP silicone oil 5000 (Dow Corning fluid). Interfacial tension 38 dyn/cm.

C.2 Figure 4: η_r vs ϕ

Datasets:

- Squares: obtained from Figure 8 in Ref. [42] for a monodisperse silicon oil-in-water emulsion with sodium dodecyl sulfate (SDS) concentration of 10 mM, droplet size $a = 0.55$ µm, viscosity of the oil $\lambda\mu = 12$ cP, water viscosity $\mu = 0.997$ cP, $\lambda = 12$, and $\sigma = 9.8$ dyn/cm.
- Circles: obtained from Figure 8 in Ref. [42] for a monodisperse silicon oil-in-water emulsion with SDS concentration of 10 mM, droplet size $a = 0.20$ µm, viscosity of the oil $\lambda\mu = 12$ cP, water viscosity $\mu = 104$ cP, $\lambda = 0.12$, and $\sigma = 9.8$ dyn/cm.
- Pentagons: obtained from Figure 6 set 2 in Ref. [231] for a polydisperse petroleum oil-in-water emulsion with Triton-X-100 concentration of 2.1 wt%. Effective drop radius $a_{32} = 9.12$ µm, viscosity of the oil $\lambda\mu = 5.52$ cP, water viscosity $\mu = 0.997$ cP, $\lambda = 5.54$, and $\sigma = 1.5$ dyn/cm.
- Triangles: obtained from Figure 6 set 2 in Ref. [231] for a polydisperse petroleum oil-in-water emulsion with Triton-X-100 concentration of 2.1 wt%. Effective drop radius $a_{32} = 9.12$ µm, viscosity of the oil $\lambda\mu = 5.52$ cP, water viscosity $\mu = 0.997$ cP, $\lambda = 5.54$, and $\sigma = 1.5$ dyn/cm.

Models:

- Taylor [11]: using Ref. [231] emulsion of oil and water viscosities $\lambda\mu = 5.52$ cP and $\mu = 0.997$ cP, respectively, and $\lambda = 5.54$.
- Choi and Schowalter [16]: using Ref. [231] emulsion of oil and water viscosities $\lambda\mu = 5.52$ cP and $\mu = 0.997$ cP, respectively, and $\lambda = 5.54$.
- Krieger−Dougherty-like: using $\phi_m = 0.64$ and $\lambda = 5.54$ according to Ref. [150]. Another line was plotted with $\lambda = 110$ from Ref. [42] to better overlap the experimental data.

C.3 Figure 7: $\overline{G}$ vs ϕ

Datasets:

- Triangles: $E(\phi)$ points extracted from Figure 6 in Ref. [203], where $E(\phi) = G\sigma/(a_{32}\phi^{1/3})$. Polydisperse paraffin oil-in-water emulsion with 11.6 wt% Alipal CD-128, 58% active. Each emulsion has an individual mean diameter and interfacial tension as follows:

Table 1

Correspondence between symbols and nomenclature used in the review and the official list of symbols and nomenclature of The Society of Rheology [232].

List of symbols		
Name	Our symbol	SoR symbol
Shear stress	τ	$\boldsymbol{\sigma}$
Yield stress	τ_Y	σ_Y
Fluid viscosity	μ	η_f
Maximum packing fraction	ϕ_m	ϕ_{max}
Local stress tensor	$\mathbf{T}$	$\boldsymbol{\sigma}(\mathbf{x}, t)$
Boussinesq number	B_q	Bo
Interfacial shear viscosity	μ_s	μ^s
Interfacial dilatational viscosity	μ_d	κ^s
Rate-of-strain tensor	$\mathbf{E}$	$\dot{\gamma}/2$ or $\mathbf{D}$

$a_{32} = 8.43 - 8.92$ μm, $\lambda\mu = 49.2$ cP, $\mu = 2.22$ cP, $\lambda = 22.2$, and $\sigma = 6.20 - 6.86$ dyn/cm.

- Circles: dataset for particle size $a = 0.53$ μm from Ref. [204] according to Figure 2(b) (black down triangles) in Ref. [8]. Monodisperse silicon oil-in-water emulsion with SDS concentration of C = 10 mM, where $\lambda\mu = 110$ cP, $\mu = 0.997$ cP, $\lambda = 110$, and $\sigma = 9.8$ dyn/cm.

Models:

- Princen and Kiss [41] model plotted in the range $\phi = 0.73 - 1$.
- Wilking and Mason [205] model plotted in the range $\phi = 0.73 - 1$; assuming $\phi_m = 0.71$.

C.4 Figure 7: $\bar{\tau}_Y$ vs ϕ

- Squares: rescaled data from Table 1 of Ref. [41]. Polydisperse paraffin oil-in-water emulsion with 10% Neodol 25-3 S + 2% Neodol 25—9. Each emulsion has an individual mean diameter and interfacial tension in the ranges: $a_{32} = 5.73 - 10.2$ μm, oil viscosity $\lambda\mu = 49.2$ cP, water viscosity $\mu = 1.53$ cP, $\lambda = 32.2$, and $\sigma = 4.50 - 4.92$ dyn/cm.
- Triangles: replotted from Figure 4 (circles) in Ref. [42]. Monodisperse silicon oil-in-water emulsion with SDS concentration of 10 mM, drop size $a = 0.25$ μm, $\lambda\mu = 12$ cP, $\mu = 104$ cP, $\lambda = 0.12$, and interfacial tension $\sigma = 9.8$ dyn/cm.
- Hexagons: replotted from Figure 4 (squares) in Ref. [42]. Monodisperse silicon oil-in-water emulsion with SDS concentration of 10 mM, drop size $a = 0.53$ μm, $\lambda\mu = 12$ cP, $\mu = 104$ cP, $\lambda = 0.12$, and interfacial tension $\sigma = 9.8$ dyn/cm.

Models:

- Princen and Kiss (1989) [41]: plotted in the range $\phi = 0.646 - 1$. Scaled with the following parameters: $a_{32} = 10.05$ μm, $\sigma = 4.723$ dyn/cm.
- Mason, Bibette, and Weitz (1996) [42]: plotted in the range $\phi = 0.646 - 1$ using the empirical quadratic fit for the scaled yield stress $\tau_Y/(\sigma/a) = 0.51(\phi_{eff} - \phi_c)^2$ where $\phi_c = 0.62$.

D. Table of symbols and nomenclature

Table 1 is like a Rosetta stone that lists the symbols used in this work against the nomenclature adopted by the Society of Rheology [232]. We have endeavored to adopt consistent symbols within the paper and introduced simplifications when possible for brevity and improving clarity.

Data availability

Data will be made available on request.

References

Papers of particular interest, published within the period of review, have been highlighted as:

* of special interest
** of outstanding interest

1. * Langevin D: Emulsions, microemulsions and foams. Springer; 2020.

2. Tadros TF: Emulsions: formation, stability, industrial applications. Walter de Gruyter GmbH & Co KG; 2016.

3. Bibette J, Leal-Calderon F, Schmitt V, Poulin P: Emulsion science: basic principles. An overview. Springer; 2003.

4. ** Larson RG. *The structure and rheology of complex fluids*. New York: Oxford University Press; 1999.

A comprehensive introduction to thermodynamics-structure-rheology of emulsions and many complex fluids (polymer solutions and melts, surfactants, particle suspensions, liquid crystals).

5. Macosko CW: *Rheology: principles, measurements and applications*. Wiley-VCH Inc; 1994.

6. Mewis J, Wagner NJ. *Colloidal suspension rheology*, **10**. Cambridge University Press; 2012.

7. ** Vlassopoulos D, Cloitre M: **Tunable rheology of dense soft deformable colloids**. *Curr Opin Colloid Interface Sci* 2014, **19**: 561–574.

8. ** Kim HS, Mason TG: **Advances and challenges in the rheology of concentrated emulsions and nanoemulsions**. *Adv Colloid Interface Sci* 2017, **247**:397–412.

9. ** Minale M: **Models for the deformation of a single ellipsoidal drop: a review**. *Rheol Acta* 2010, **49**:789–806.

10. Barnes HA: **Rheology of emulsions—a review**. *Colloids Surf A Physicochem Eng Asp* 1994, **91**:89–95.

11. ** Taylor GI: **The viscosity of a fluid containing small drops of another fluid**. *Proc R Soc Lond - Ser A Contain Pap a Math Phys Character* 1932, **138**:41–48.

12. ** Oldroyd J: **The elastic and viscous properties of emulsions and suspensions**. *Proc Roy Soc Lond Math Phys Sci* 1953, **218**: 122–132.

13. Schowalter W, Chaffey C, Brenner H: **Rheological behavior of a dilute emulsion**. *J Colloid Interface Sci* 1968, **26**: 152–160.

14. * Cox R: **The deformation of a drop in a general time-dependent fluid flow**. *J Fluid Mech* 1969, **37**:601–623.

15. * * Frankel N, Acrivos A: **The constitutive equation for a dilute emulsion**. *J Fluid Mech* 1970, **44**:65–78.

16. * * Choi SJ, Schowalter W: **Rheological properties of nondilute suspensions of deformable particles**. *Phys Fluids* 1975, **18**: 420–427.

17. Langevin D: **Influence of interfacial rheology on foam and emulsion properties**. *Adv Colloid Interface Sci* 2000, **88**: 209–222.

18. * Erni P, Windhab EJ, Fischer P: **Emulsion drops with complex interfaces: globular versus flexible proteins**. *Macromol Mater Eng* 2011, **296**:249–262.

19. * * Erni P: **Deformation modes of complex fluid interfaces**. *Soft Matter* 2011, **7**:7586–7600.

Excellent starting point for learning about interfacial rheology.

20. * * Fischer P, Erni P: **Emulsion drops in external flow fields—the role of liquid interfaces**. *Curr Opin Colloid Interface Sci* 2007, **12**:196–205.

21. * * Flumerfelt RW: **Effects of dynamic interfacial properties on drop deformation and orientation in shear and extensional flow fields**. *J Colloid Interface Sci* 1980, **76**:330–349.

22. * Derkach SR: **Rheology of emulsions**. *Adv Colloid Interface Sci* 2009, **151**:1–23.

23. * Foudazi R, Qavi S, Masalova I, Malkin AY: **Physical chemistry of highly concentrated emulsions**. *Adv Colloid Interface Sci* 2015, **220**:78–91.

24. Pal R: **Rheology of simple and multiple emulsions**. *Curr Opin Colloid Interface Sci* 2011, **16**:41–60.

25. Huisman F, Friedman S, Taborek P: **Pinch-off dynamics in foams, emulsions and suspensions**. *Soft Matter* 2012, **8**: 6767–6774.

26. Niedzwiedz K, Buggisch H, Willenbacher N: **Extensional rheology of concentrated emulsions as probed by capillary breakup elongational rheometry (caber)**. *Rheol Acta* 2010, **49**: 1103–1116.

27. Dinic J, Jimenez LN, Sharma V: **Pinch-off dynamics and dripping-onto-substrate (dos) rheometry of complex fluids**. *Lab Chip* 2017, **17**:460–473.

28. Nikolova NN, Narváez CDM, Hassan L, Nicholson RA, Boehm MW, Baier SK, Sharma V: **Rheology and dispensing of real and vegan mayo: the chickpea or egg problem**. *Soft Matter* 2023, **19**:9413–9427.

29. * * Torza S, Cox R, Mason S: **Particle motions in sheared suspensions xxvii. transient and steady deformation and burst of liquid drops**. *J Colloid Interface Sci* 1972, **38**: 395–411.

Excellent discussion of theory and experiments on deformation and breakup of drops.

30. Stone HA, Bentley B, Leal L: **An experimental study of transient effects in the breakup of viscous drops**. *J Fluid Mech* 1986, **173**:131–158.

31. * Bentley B, Leal LG: **An experimental investigation of drop deformation and breakup in steady, two-dimensional linear flows**. *J Fluid Mech* 1986, **167**:241–283.

32. * * Rallison J: **The deformation of small viscous drops and bubbles in shear flows**. *Annu Rev Fluid Mech* 1984, **16**: 45–66.

Comprehensive, insightful, and incisive review of deformation under flow.

33. Vankova N, Tcholakova S, Denkov ND, Ivanov IB, Vulchev VD, Danner T: **Emulsification in turbulent flow: 1. mean and maximum drop diameters in inertial and viscous regimes**. *J Colloid Interface Sci* 2007, **312**:363–380.

34. Vankova N, Tcholakova S, Denkov ND, Vulchev VD, Danner T: **Emulsification in turbulent flow: 2. breakage rate constants**. *J Colloid Interface Sci* 2007, **313**:612–629.

35. Ni R: **Deformation and breakup of bubbles and drops in turbulence**. *Annu Rev Fluid Mech* 2024, **56**:319–347.

36. DeRoussel P, Khakhar D, Ottino J: **Mixing of viscous immiscible liquids. part 1: computational models for strong–weak and continuous flow systems**. *Chem Eng Sci* 2001, **56**: 5511–5529.

37. * Fardin MA, Hautefeuille M, Sharma V: **Spreading, pinching, and coalescence: the ohnesorge units**. *Soft Matter* 2022, **18**: 3291–3303.

38. * * Fardin MA, Hautefeuille M, Sharma V: **Dynamic duos: the building blocks of dimensional mechanics**. *Soft Matter* 2024: 5475–5508.

Dimensional analysis presented with unique and extensive insights into mechanics.

39. Doi M, Edwards SF. *The theory of polymer dynamics*. Oxford University Press; 1988.

40. Vermant J, Van Puyvelde P, Moldenaers P, Mewis J, Fuller G: **Anisotropy and orientation of the microstructure in viscous emulsions during shear flow**. *Langmuir* 1998, **14**:1612–1617.

41. * * Princen H, Kiss A: **Rheology of foams and highly concentrated emulsions: IV an experimental study of the shear viscosity and yield stress of concentrated emulsions**. *J Colloid Interface Sci* 1989, **128**:176–187.

42. Mason T, Bibette J, Weitz D: **Yielding and flow of monodisperse emulsions**. *J Colloid Interface Sci* 1996, **179**:439–448.

43. * Larson R: **The elastic stress in "film fluids,"**. *J Rheol* 1997, **41**: 365–372.

44. Cohen-Addad S, Höhler R: **Rheology of foams and highly concentrated emulsions**. *Curr Opin Colloid Interface Sci* 2014, **19**:536–548.

45. * * Guido S: **Shear-induced droplet deformation: effects of confined geometry and viscoelasticity**. *Curr Opin Colloid Interface Sci* 2011, **16**:61–70.

Essential references for quick overview of how confinement and non-Newtonian nature of the either liquid phases.

46. McClements DJ, Bai L, Chung C: **Recent advances in the utilization of natural emulsifiers to form and stabilize emulsions**. *Annu Rev Food Sci Technol* 2017, **8**:205–236.

47. Zhu Y, Gao H, Liu W, Zou L, McClements DJ: **A review of the rheological properties of dilute and concentrated food emulsions**. *J Texture Stud* 2020, **51**:45–55.

48. Esquena J: **Water-in-water (w/w) emulsions**. *Curr Opin Colloid Interface Sci* 2016, **25**:109–119.

49. Fick C, Khan Z, Srivastava S: **Interfacial stabilization of aqueous two-phase systems: a review**. *Materials Advances* 2023.

50. Helgeson ME: **Colloidal behavior of nanoemulsions: interactions, structure, and rheology**. *Curr Opin Colloid Interface Sci* 2016, **25**:39–50.

51. Gupta A, Badruddoza AZM, Doyle PS: **A general route for nanoemulsion synthesis using low-energy methods at constant temperature**. *Langmuir* 2017, **33**:7118–7123.

52. McClements DJ: **Nanoemulsions versus microemulsions: terminology, differences, and similarities**. *Soft Matter* 2012, **8**: 1719–1729.

53. Sanfeld A, Steinchen A: **Emulsions stability, from dilute to dense emulsions—role of drops deformation**. *Adv Colloid Interface Sci* 2008, **140**:1–65.

54. * * Morris JF: **Shear thickening of concentrated suspensions: recent developments and relation to other phenomena**. *Annu Rev Fluid Mech* 2020, **52**:121–144.

55. Singh A, Ness C, Seto R, de Pablo JJ, Jaeger HM: **Shear thickening and jamming of dense suspensions: the "roll" of friction**. *Phys Rev Lett* 2020, **124**, 248005.

56. Datta SS, Gerrard DD, Rhodes TS, Mason TG, Weitz DA: **Rheology of attractive emulsions, physical review E—statistical, nonlinear, and**. *Soft Matter Physics* 2011, **84**, 041404.

57. Cao C, Liao J, Breedveld V, Weeks ER: **Rheology finds distinct glass and jamming transitions in emulsions**. *Soft Matter* 2021, **17**:2587–2595.

58. ** Chaffey CE, Brenner H: **A second-order theory for shear deformation of drops**. *J Colloid Interface Sci* 1967, **24**: 258–269.

59. ** Ramachandran A, Gary Leal L: **The effect of interfacial slip on the rheology of a dilute emulsion of drops for small capillary numbers**. *J Rheol* 2012, **56**:1555–1587.

60. * Narsimhan V: **Shape and rheology of droplets with viscous surface moduli**. *J Fluid Mech* 2019, **862**:385–420.

61. Einstein A: **Eine neue bestimmung der molekuldimensionen**. *Ann Phys* 1906, **324**:289–306.

62. ** Einstein A: **Berichtigung zu meiner arbeit: Eine neue bestimmung der molekuldimensionen**. *Ann Phys* 1911, **339**:591–592.

63. ** Barthès-Biesel D, Acrivos A: **The rheology of suspensions and its relation to phenomenological theories for non-Newtonian fluids**. *Int J Multiphas Flow* 1973, **1**:1–24.

64. Stone HA, Leal LG: **The effects of surfactants on drop deformation and breakup**. *J Fluid Mech* 1990, **220**:161–186.

65. Barthès-Biesel D: **Motion of a spherical microcapsule freely suspended in a linear shear flow**. *J Fluid Mech* 1980, **100**: 831–853.

66. Barthès-Biesel D, Rallison J: **The time-dependent deformation of a capsule freely suspended in a linear shear flow**. *J Fluid Mech* 1981, **113**:251–267.

67. * Barthès-Biesel D: **Modeling the motion of capsules in flow**. *Curr Opin Colloid Interface Sci* 2011, **16**:3–12.

68. ** Barthès-Biesel D: **Motion and deformation of elastic capsules and vesicles in flow**. *Annu Rev Fluid Mech* 2016, **48**:25–52.

69. ** Oldroyd J: **The effect of interfacial stabilizing films on the elastic and viscous properties of emulsions**. *Proc Roy Soc Lond Math Phys Sci* 1955, **232**:567–577.

70. * Fröhlich A, Sack R: **Theory of the rheological properties of dispersions**. *Proc Roy Soc Lond Math Phys Sci* 1946, **185**: 415–430.

71. Mwasame PM, Wagner NJ, Beris AN: **On the macroscopic modelling of dilute emulsions under flow**. *J Fluid Mech* 2017, **831**:433–473.

72. Pal R: **Rheology of polymer-thickened emulsions**. *J Rheol* 1992, **36**:1245–1259.

73. * Kennedy MR, Pozrikidis C, Skalak R: **Motion and deformation of liquid drops, and the rheology of dilute emulsions in simple shear flow**. *Comput Fluid* 1994, **23**:251–278.

74. Li X, Pozrikidis C: **The effect of surfactants on drop deformation and on the rheology of dilute emulsions in Stokes flow**. *J Fluid Mech* 1997, **341**:165–194.

75. * Guido S, Greco F, *et al.*: **Dynamics of a liquid drop in a flowing immiscible liquid**. *Rheology Reviews* 2004:99–142.

76. Aggarwal N, Sarkar K: **Rheology of an emulsion of viscoelastic drops in steady shear**. *J Non-Newtonian Fluid Mech* 2008, **150**: 19–31.

77. ** Vlahovska PM, Bławzdziewicz J, Loewenberg M: **Small-deformation theory for a surfactant-covered drop in linear flows**. *J Fluid Mech* 2009, **624**:293–337.

78. * Oliveira TF, da Cunha FR: **Emulsion rheology for steady and oscillatory shear flows at moderate and high viscosity ratio**. *Rheol Acta* 2015, **54**:951–971.

79. Escott LJ, Wilson HJ: **Rheology of a suspension of deformable spheres in a weakly viscoelastic fluid**. *J Non-Newtonian Fluid Mech* 2024, 105262.

80. Villone MM, Maffettone PL: **Dynamics, rheology, and applications of elastic deformable particle suspensions: a review**. *Rheol Acta* 2019, **58**:109–130.

81. Miksis MJ: **Shape of a drop in an electric field**. *Phys Fluids* 1981, **24**:1967–1972.

82. Cristini V, Tan Y-C: **Theory and numerical simulation of droplet dynamics in complex flows—a review**. *Lab Chip* 2004, **4**:257–264.

83. Bazhlekov IB, Anderson PD, Meijer HE: **Numerical investigation of the effect of insoluble surfactants on drop deformation and breakup in simple shear flow**. *J Colloid Interface Sci* 2006, **298**:369–394.

84. Vananroye A, Janssen PJ, Anderson PD, Van Puyvelde P, Moldenaers P: **Microconfined equiviscous droplet deformation: comparison of experimental and numerical results**. *Phys Fluids* 2008, **20**.

85. Janssen P, Vananroye A, Van Puyvelde P, Moldenaers P, Anderson P: **Generalized behavior of the breakup of viscous drops in confinements**. *J Rheol* 2010, **54**:1047–1060.

86. Cunha LH, Siqueira IR, Oliveira TF, Ceniceros HD: **Field-induced control of ferrofluid emulsion rheology and droplet break-up in shear flows**. *Phys Fluids* 2018, **30**.

87. Roure G, Zinchenko AZ, Davis RH: **Numerical simulation of deformable droplets in three-dimensional, complex-shaped microchannels**. *Phys Fluids* 2023, **35**.

88. Rallison J: **Note on the time-dependent deformation of a viscous drop which is almost spherical**. *J Fluid Mech* 1980, **98**: 625–633.

89. Kibbelaar HM, Deblais A, Briand G, Hendrix Y, Gaillard A, Velikov K, Denn M, Bonn D: **Towards a constitutive relation for emulsions exhibiting a yield stress**. *Physical Review Fluids* 2023, **8**, 123301.

90. Hermes M, Clegg PS: **Yielding and flow of concentrated pickering emulsions**. *Soft Matter* 2013, **9**:7568–7575.

91. Dardelle G, Erni P: **Three-phase interactions and interfacial transport phenomena in coacervate/oil/water systems**. *Adv Colloid Interface Sci* 2014, **206**:79–91.

92. Erni P, Fischer P, Windhab EJ: **Role of viscoelastic interfaces in emulsion rheology and drop deformation**. *J Cent S Univ Technol* 2007, **14**:246–249.

93. Erni P, Fischer P, Windhab EJ: **Deformation of single emulsion drops covered with a viscoelastic adsorbed protein layer in simple shear flow**. *Appl Phys Lett* 2005, **87**.

94. Sharma V, Jaishankar A, Wang Y-C, McKinley GH: **Rheology of globular proteins: apparent yield stress, high shear rate viscosity and interfacial viscoelasticity of bovine serum albumin solutions**. *Soft Matter* 2011, **7**:5150–5160.

95. Edwards DA, Brenner H, Wasan DT: Interfacial transport processes and rheology. Butterworth-Heinemann; 1967.

96. Chatzigiannakis E, Jaensson N, Vermant J: **Thin liquid films: where hydrodynamics, capillarity, surface stresses and intermolecular forces meet**. *Curr Opin Colloid Interface Sci* 2021, **53**, 101441.

97. ** Loewenberg M: **Numerical simulation of concentrated emulsion flows**. *J Fluid Eng* 1998, **120**:824–832.

98. Stone HA: **A simple derivation of the time-dependent convective-diffusion equation for surfactant transport along a deforming interface**. *Phys Fluids* 1990, **2**:111–112.

99. Eggleton CD, Stebe KJ: **An adsorption–desorption-controlled surfactant on a deforming droplet**. *J Colloid Interface Sci* 1998, **208**:68–80.

100. ** Manikantan H, Squires TM: **Surfactant dynamics: hidden variables controlling fluid flows**. *J Fluid Mech* 2020, **892**:P1.
State-of-the-art detailed review on influence of surfactants on interfacial flows.

101. Eggleton CD, Pawar YP, Stebe KJ: **Insoluble surfactants on a drop in an extensional flow: a generalization of the stagnated**

surface limit to deforming interfaces. *J Fluid Mech* 1999, **385**: 79–99.

102. Leal LG. *Advanced transport phenomena: fluid mechanics and convective transport processes*. Cambridge University Press; 2007.

103. Håkansson A: **Emulsion formation by homogenization: current understanding and future perspectives**. *Annu Rev Food Sci Technol* 2019, **10**:239–258.

104. Håkansson A, Nilsson L: **Emulsifier adsorption kinetics influences drop deformation and breakup in turbulent emulsification**. *Soft Matter* 2023, **19**:9059–9073.

105. Schwalbe JT, Phelan Jr FR, Vlahovska PM, Hudson SD: **Interfacial effects on droplet dynamics in Poiseuille flow**. *Soft Matter* 2011, **7**:7797–7804.

106. ** Jaensson NO, Anderson PD, Vermant J: **Computational interfacial rheology**. *J Non-Newtonian Fluid Mech* 2021, **290**:104507.

107. Pozrikidis C: **Effects of surface viscosity on the finite deformation of a liquid drop and the rheology of dilute emulsions in simple shearing flow**. *J Non-Newtonian Fluid Mech* 1994, **51**: 161–178.

108. Luo ZY, Shang XL, Bai BF: **Influence of pressure-dependent surface viscosity on dynamics of surfactant-laden drops in shear flow**. *J Fluid Mech* 2019, **858**:91–121.

109. Herrada MA, Ponce-Torres A, Rubio M, Eggers J, Montanero JM: **Stability and tip streaming of a surfactant-loaded drop in an extensional flow. influence of surface viscosity**. *J Fluid Mech* 2022, **934**:A26.

110. Kim K, Choi SQ, Zasadzinski JA, Squires TM: **Interfacial microrheology of dppc monolayers at the air–water interface**. *Soft Matter* 2011, **7**:7782–7789.

111. Kim K, Choi SQ, Zell ZA, Squires TM, Zasadzinski JA: **Effect of cholesterol nanodomains on monolayer morphology and dynamics**. *Proc Natl Acad Sci USA* 2013, **110**:E3054–E3060.

112. Samaniuk JR, Vermant J: **Micro and macrorheology at fluid–fluid interfaces**. *Soft Matter* 2014, **10**:7023–7033.

113. Hermans E, Vermant J: **Interfacial shear rheology of dppc under physiologically relevant conditions**. *Soft Matter* 2014, **10**:175–186.

114. Falavarjani AR, Salac D: **Modeling droplets with slippery interfaces**. *J Comput Phys* 2023, **481**, 112033.

115. * Cardinaels R, Moldenaers P: **Morphology development in immiscible polymer blends**. *Polymer Morphology: Principles, Characterization, and Processing* 2016:348–373.

116. * Greco F: **Drop deformation for non-Newtonian fluids in slow flows**. *J Non-Newtonian Fluid Mech* 2002, **107**:111–131.

117. Batchelor GK: An introduction to fluid dynamics. Cambridge University Press; 1991.

118. ** Batchelor G: **The stress system in a suspension of force-free particles**. *J Fluid Mech* 1970, **41**:545–570.
Both small and large deformation modes are discussed.

119. Bird RB, Armstrong RC, Hassager O: Dynamics of polymeric liquids. Vol. 1: fluid mechanics. New York, NY: John Wiley and Sons Inc.; 1987.

120. ** Stone HA: **Dynamics of drop deformation and breakup in viscous fluids**. *Annu Rev Fluid Mech* 1994, **26**:65–102.

121. Rallison J, Acrivos A: **A numerical study of the deformation and burst of a viscous drop in an extensional flow**. *J Fluid Mech* 1978, **89**:191–200.

122. Cristini V, Bławzdziewicz J, Loewenberg M: **An adaptive mesh algorithm for evolving surfaces: simulations of drop breakup and coalescence**. *J Comput Phys* 2001, **168**:445–463.

123. Milliken W, Stone HA, Leal L: **The effect of surfactant on the transient motion of Newtonian drops**. *Phys Fluid* 1993, **5**: 69–79.

124. Eggleton CD, Tsai T-M, Stebe KJ: **Tip streaming from a drop in the presence of surfactants**. *Phys Rev Lett* 2001, **87**, 048302.

125. James AJ, Lowengrub J: **A surfactant-conserving volume-of-fluid method for interfacial flows with insoluble surfactant**. *J Comput Phys* 2004, **201**:685–722.

126. Lee J, Pozrikidis C: **Effect of surfactants on the deformation of drops and bubbles in Navier–Stokes flow**. *Comput Fluid* 2006, **35**:43–60.

127. Xu J-J, Li Z, Lowengrub J, Zhao H: **A level-set method for interfacial flows with surfactant**. *J Comput Phys* 2006, **212**: 590–616.

128. Muradoglu M, Tryggvason G: **A front-tracking method for computation of interfacial flows with soluble surfactants**. *J Comput Phys* 2008, **227**:2238–2262.

129. Pimenta PHN, Oliveira TFd: **Study on the rheology of a dilute emulsion of surfactant-covered droplets using the level set and closest point methods**. *Phys Fluids* 2021, **33**.

130. Gounley J, Boedec G, Jaeger M, Leonetti M: **Influence of surface viscosity on droplets in shear flow**. *J Fluid Mech* 2016, **791**:464–494.

131. Singh N, Narsimhan V: **Deformation and burst of a liquid droplet with viscous surface moduli in a linear flow field**. *Physical Review Fluids* 2020, **5**, 063601.

132. Singh N, Narsimhan V: **Impact of surface rheology on droplet coalescence in uniaxial compressional flow**. *Physical Review Fluids* 2023, **8**, 083602.

133. Williams A, Janssen J, Prins A: **Behaviour of droplets in simple shear flow in the presence of a protein emulsifier**. *Colloids Surf A Physicochem Eng Asp* 1997, **125**:189–200.

134. ** Taylor GI: **The formation of emulsions in definable fields of flow**. *Proc R Soc Lond - Ser A Contain Pap a Math Phys Character* 1934, **146**:501–523.

135. Cristini V, Guido S, Alfani A, Bławzdziewicz J, Loewenberg M: **Drop breakup and fragment size distribution in shear flow**. *J Rheol* 2003, **47**:1283–1298.

136. Rumscheidt F-D, Mason S: **Particle motions in sheared suspensions xii. deformation and burst of fluid drops in shear and hyperbolic flow**. *J Colloid Sci* 1961, **16**:238–261.

137. De Bruijn R: **Tipstreaming of drops in simple shear flows**. *Chem Eng Sci* 1993, **48**:277–284.

138. ** Grace HP: **Dispersion phenomena in high viscosity immiscible fluid systems and application of static mixers as dispersion devices in such systems**. *Chem Eng Commun* 1982, **14**:225–277.

139. Dinic J, Sharma V: **Macromolecular relaxation, strain, and extensibility determine elastocapillary thinning and extensional viscosity of polymer solutions**. *Proc Natl Acad Sci USA* 2019, **116**:8766–8774.

140. Mukherjee S, Sarkar K: **Effects of viscosity ratio on deformation of a viscoelastic drop in a Newtonian matrix under steady shear**. *J Non-Newtonian Fluid Mech* 2009, **160**:104–112.

141. Acrivos A, Lo T: **Deformation and breakup of a single slender drop in an extensional flow**. *J Fluid Mech* 1978, **86**:641–672.

142. Ramaswamy S, Leal L: **The deformation of a Newtonian drop in the uniaxial extensional flow of a viscoelastic liquid**. *J Non-Newtonian Fluid Mech* 1999, **88**:149–172.

143. Ramaswamy S, Leal L: **The deformation of a viscoelastic drop subjected to steady uniaxial extensional flow of a Newtonian fluid**. *J Non-Newtonian Fluid Mech* 1999, **85**:127–163.

144. Milliken W, Leal L: **Deformation and breakup of viscoelastic drops in planar extensional flows**. *J Non-Newtonian Fluid Mech* 1991, **40**:355–379.

145. Spencer AJM: *Continuum mechanics*. Courier Corporation; 2004.

146.* Barthès-Biesel D, Acrivos A: **Deformation and burst of a liquid droplet freely suspended in a linear shear field**. *J Fluid Mech* 1973, **61**:1–22.

147. Utracki L: **Melt flow of polymer blends**. *Polym Eng Sci* 1983, **23**: 602–609.

148.* Yaron I, Gal-Or B: **On viscous flow and effective viscosity of concentrated suspensions and emulsions: effect of particle concentration and surfactant impurities**. *Rheol Acta* 1972, **11**: 241–252.

149.* Palierne J: **Linear rheology of viscoelastic emulsions with interfacial tension**. *Rheol Acta* 1990, **29**:204–214.

150. Pal R: **Novel viscosity equations for emulsions of two immiscible liquids**. *J Rheol* 2001, **45**:509–520.

151. Pal R: **Recent developments in the viscosity modeling of concentrated monodisperse emulsions**. *Foods* 2023, **12**:3483.

152.* * Maffettone P, Minale M: **Equation of change for ellipsoidal drops in viscous flow**. *J Non-Newtonian Fluid Mech* 1998, **78**: 227–241.

153.* Taylor G: **Conical free surfaces and fluid interfaces**. In *Applied mechanics: proceedings of the eleventh international congress of applied mechanics Munich (Germany) 1964*. Springer; 1966: 790–796.

154. Khakhar D, Ottino J: **Deformation and breakup of slender drops in linear flows**. *J Fluid Mech* 1986, **166**:265–285.

155. Hinch EJ, Acrivos A: **Long slender drops in a simple shear flow**. *J Fluid Mech* 1980, **98**:305–328.

156.* * Doi M, Ohta T: **Dynamics and rheology of complex interfaces. i**. *J Chem Phys* 1991, **95**:1242–1248.

157.* * Tucker III CL, Moldenaers P: **Microstructural evolution in polymer blends**. *Annu Rev Fluid Mech* 2002, **34**:177–210.

158. Loewenberg M, Hinch EJ: **Collision of two deformable drops in shear flow**. *J Fluid Mech* 1997, **338**:299–315.

159. Kim J, Lowengrub J: **Interfaces and multicomponent fluids**. *Encyclopedia of Mathematical Physics* 2004:135–144.

160.* * Prosperetti A, Tryggvason G: Computational methods for multiphase flow. Cambridge University Press; 2009.

161.* * Pozrikidis C: Boundary integral and singularity methods for linearized viscous flow. Cambridge University Press; 1992.

162. Peskin CS: **The immersed boundary method**. *Acta Numer* 2002, **11**:479–517.

163. Hirt CW, Nichols BD: **Volume of fluid (vof) method for the dynamics of free boundaries**. *J Comput Phys* 1981, **39**: 201–225.

164.* Cahn JW, Hilliard JE: **Free energy of a nonuniform system. i. interfacial free energy**. *J Chem Phys* 1958, **28**:258–267.

165. Osher S, Fedkiw R, Piechor K: **Level set methods and dynamic implicit surfaces**. *Appl Mech Rev* 2004, **57**:B15. –B15.

166. Gibou F, Fedkiw R, Osher S: **A review of level-set methods and some recent applications**. *J Comput Phys* 2018, **353**: 82–109.

167.* * Anthony CR, Wee H, Garg V, Thete SS, Kamat PM, Wagoner BW, Wilkes ED, Notz PK, Chen AU, Suryo R, *et al.*: **Sharp interface methods for simulation and analysis of free surface flows with singularities: breakup and coalescence**. *Annu Rev Fluid Mech* 2023, **55**:707–747.

168. Kistler S, Scriven LE: **Coating flow theory by finite element and asymptotic analysis of the Navier-Stokes system**. *Int J Numer Methods Fluid* 1984, **4**:207–229.

169.* Basaran OA: **Small-scale free surface flows with breakup: drop formation and emerging applications**. *AIChE J* 2002, **48**: 1842.

170. Tryggvason G, Scardovelli R, Zaleski S: Direct numerical simulations of gas–liquid multiphase flows. Cambridge University Press; 2011.

171. Hu W-F, Lai M-C, Young Y-N: **A hybrid immersed boundary and immersed interface method for electrohydrodynamic simulations**. *J Comput Phys* 2015, **282**:47–61.

172. Hoogerbrugge P, Koelman J: **Simulating microscopic hydrodynamic phenomena with dissipative particle dynamics**. *Europhys Lett* 1992, **19**:155.

173. Krüger T, Kusumaatmaja H, Kuzmin A, Shardt O, Silva G, Viggen EM: The Lattice Boltzmann method: principles and practice. Springer; 2017.

174.* * Loewenberg M, Hinch EJ: **Numerical simulation of a concentrated emulsion in shear flow**. *J Fluid Mech* 1996, **321**: 395–419.

175.* * Zinchenko AZ, Davis RH: **Shear flow of highly concentrated emulsions of deformable drops by numerical simulations**. *J Fluid Mech* 2002, **455**:21–61.

176. Zinchenko AZ, Davis RH: **General rheology of highly concentrated emulsions with insoluble surfactant**. *J Fluid Mech* 2017, **816**:661–704.

177. Zinchenko AZ, Gissinger JR, Davis RH: **Flow of a concentrated emulsion with surfactant through a periodic porous medium**. *J Fluid Mech* 2022, **953**, A21.

178. Girotto I, Scagliarini A, Benzi R, Toschi F: **Lagrangian statistics of concentrated emulsions**. *J Fluid Mech* 2024, **986**, A33.

179. Negro G, Carenza LN, Gonnella G, Mackay F, Morozov A, Marenduzzo D: **Yield-stress transition in suspensions of deformable droplets**. *Sci Adv* 2023, **9**, eadf8106.

180. De Vita F, Rosti ME, Caserta S, Brandt L: **Numerical simulations of vorticity banding of emulsions in shear flows**. *Soft Matter* 2020, **16**:2854–2863.

181. Rosti ME, De Vita F, Brandt L: **Numerical simulations of emulsions in shear flows**. *Acta Mech* 2019, **230**:667–682.

182. Pan D, Phan-Thien N, Khoo BC: **Dissipative particle dynamics simulation of droplet suspension in shear flow at low capillary number**. *J Non-Newtonian Fluid Mech* 2014, **212**: 63–72.

183.* * Zinchenko AZ, Davis RH: **Extensional and shear flows, and general rheology of concentrated emulsions of deformable drops**. *J Fluid Mech* 2015, **779**:197–244.

184. Zinchenko AZ, Davis RH: **An efficient algorithm for hydrodynamical interaction of many deformable drops**. *J Comput Phys* 2000, **157**:539–587.

185. Sorgentone C, Tornberg A-K: **A highly accurate boundary integral equation method for surfactant-laden drops in 3d**. *J Comput Phys* 2018, **360**:167–191.

186. Van Puyvelde P, Vananroye A, Cardinaels R, Moldenaers P: **Review on morphology development of immiscible blends in confined shear flow**. *Polymer* 2008, **49**: 5363–5372.

187. Kapiamba KF: **Mini-review of the microscale phenomena during emulsification of highly concentrated emulsions**. *Colloid and Interface Science Communications* 2022, **47**, 100597.

188. Santos RGd: *Concentrated ferrofluid emulsions under shear flow and uniform magnetic fields*. University of Brasilia; 2024. Master's thesis.

189. Rosti ME, Takagi S: **Shear-thinning and shear-thickening emulsions in shear flows**. *Phys Fluids* 2021, **33**.

190. Wang N, Ni W, Wang D, Liu H: **Deformation and breakup behaviors of a giesekus viscoelastic droplet in Newtonian shear flow**. *Comput Fluid* 2023, **263**, 105970.

191. Zhang H, Gong W, Yuan W, Meng B: **Numerical investigation on the deformation and breakup of an elastoviscoplastic droplet in simple shear flow**. *Phys Fluids* 2024, **36**.

192. Caserta S, Guido S: **Vorticity banding in biphasic polymer blends**. *Langmuir* 2012, **28**:16254–16262.

193. Silva DP, Coelho RC, Pagonabarraga I, Succi S, da Gama MMT, Araújo NA: **Lattice Boltzmann simulation of deformable fluid-filled bodies: progress and perspectives**. *Soft Matter* 2024.

194. Peterson J, Bagkeris I, Michael V: *A viscoelastic model for droplet breakup in dense emulsions*. 2023. arXiv preprint arXiv: 2305.16767.

195. Mason TG: **New fundamental concepts in emulsion rheology**. *Curr Opin Colloid Interface Sci* 1999, **4**:231–238.

196. Princen H: **Rheology of foams and highly concentrated emulsions: I. elastic properties and yield stress of a cylindrical model system**. *J Colloid Interface Sci* 1983, **91**:160–175.

197. ** Bonn D, Denn MM, Berthier L, Divoux T, Manneville S: **Yield stress materials in soft condensed matter**. *Rev Mod Phys* 2017, **89**, 035005.

198. * Cates M, Sollich P: **Tensorial constitutive models for disordered foams, dense emulsions, and other soft nonergodic materials**. *J Rheol* 2004, **48**:193–207.

199. Nelson AZ, Schweizer KS, Rauzan BM, Nuzzo RG, Vermant J, Ewoldt RH: **Designing and transforming yield-stress fluids**. *Curr Opin Solid State Mater Sci* 2019, **23**, 100758.

200. Geffrault A, Bessaies-Bey H, Roussel N, Coussot P: **Extensional gravity-rheometry (egr) for yield stress fluids**. *J Rheol* 2021, **65**:887–901.

201. Nicolas A, Ferrero EE, Martens K, Barrat J-L: **Deformation and flow of amorphous solids: insights from elastoplastic models**. *Rev Mod Phys* 2018, **90**, 045006.

202. Clara-Rahola J, Brzinski T, Semwogerere D, Feitosa K, Crocker J, Sato J, Breedveld V, Weeks ER: **Affine and nonaffine motions in sheared polydisperse emulsions**. *Phys Rev* 2015, **91**, 010301.

203. * Princen H, Kiss A: **Rheology of foams and highly concentrated emulsions: iii. static shear modulus**. *J Colloid Interface Sci* 1986, **112**:427–437.

204. Lacasse M-D, Grest GS, Levine D, Mason T, Weitz D: **Model for the elasticity of compressed emulsions**. *Phys Rev Lett* 1996, **76**:3448.

205. ** Wilking JN, Mason TG: **Irreversible shear-induced vitrification of droplets into elastic nanoemulsions by extreme rupturing, Physical Review E—statistical, Nonlinear, and**. *Soft Matter Physics* 2007, **75**, 041407.

206. Denkov N, Tcholakova S, Golemanov K, Ananthapadmanabhan K, Lips A: **Viscous friction in foams and concentrated emulsions under steady shear**. *Phys Rev Lett* 2008, **100**, 138301.

207. Tcholakova S, Denkov N, Golemanov K, Ananthapadmanabhan K, Lips A: **Theoretical model of viscous friction inside steadily sheared foams and concentrated emulsions**. *Phys Rev* 2008, **78**, 011405.

208. Leighton D, Acrivos A: **The shear-induced migration of particles in concentrated suspensions**. *J Fluid Mech* 1987, **181**: 415–439.

209. Leighton DT, Acrivos A: **Measurement of shear-induced self-diffusion in concentrated suspensions of spheres**. *J Fluid Mech* 1987, **177**:109–131.

210. Smart JR, Leighton DT: **Measurement of the hydrodynamic surface roughness of noncolloidal spheres**. *Phys Fluid Fluid Dynam* 1989, **1**:52–60.

211. Phillips RJ, Armstrong RC, Brown RA, Graham AL, Abbott JR: **A constitutive equation for concentrated suspensions that accounts for shear-induced particle migration**. *Phys Fluids* 1992, **4**:30.

212. Nott PR, Brady JF: **Pressure-driven flow of suspensions: simulation and theory**. *J Fluid Mech* 1994, **275**:157–199.

213. da Cunha FR, Hinch EJ: **Shear-induced dispersion in a dilute suspension of rough spheres**. *J Fluid Mech* 1996, **309**: 211–223.

214. Narsimham V, Zhao H, Shaqfeh ESG: **Coarse-grained theory to predict the concentration distribution of red blood cells in wall-bounded Couette flow at zero Reynolds number**. *Phys Fluids* 2013, **25**, 061901.

215. Rivera RGH, Zhang X, Graham MD: **Mechanistic theory of margination and flow-induced segregation in confined multicomponent suspensions: simple shear and Poiseuille flows**. *Physical Review Fluids* 2016, **1**, 060501.

216. Qi QM, Shaqfeh ESG: **Theory to predict particle migration and margination in the pressure-driven channel flow of blood**. *Physical Review Fluids* 2017, **2**, 093102.

217. Reboucas RB, Zinchenko AZ, Loewenberg M: **A pairwise hydrodynamic theory for flow-induced particle transport in shear and pressure-driven flows**. *J Fluid Mech* 2022, **952**:A2.

218. Delaby I, Muller R, Ernst B: **Drop deformation during elongational flow in blends of viscoelastic fluids. small deformation theory and comparison with experimental results**. *Rheol Acta* 1995, **34**:525–533.

219. Langevin D: **Motion of small bubbles and drops in viscoelastic fluids**. *Curr Opin Colloid Interface Sci* 2022, **57**, 101529.

220. Neo BS, Shaqfeh ES: **The effects of suspending fluid viscoelasticity on the mechanical properties of capsules and red blood cells in flow**. *J Non-Newtonian Fluid Mech* 2024, **326**, 105215.

221. Ohie K, Tasaka Y, Murai Y: **Rheology of dilute bubble suspensions in unsteady shear flows**. *J Fluid Mech* 2024, **983**:A39.

222. Mitrou S, Migliozzi S, Mazzei L, Angeli P: **On the linear viscoelastic behavior of semidilute polydisperse bubble suspensions in Newtonian media**. *J Rheol* 2024, **68**: 539–552.

223. Rust A, Manga M: **Bubble shapes and orientations in low re simple shear flow**. *J Colloid Interface Sci* 2002, **249**:476–480.

224. * Rust A, Manga M: **Effects of bubble deformation on the viscosity of dilute suspensions**. *J Non-Newtonian Fluid Mech* 2002, **104**:53–63.

225. Llewellin E, Mader H, Wilson S: **The rheology of a bubbly liquid**. *Proceedings of the Royal Society of London. Series A: Math Phys Eng Sci* 2002, **458**:987–1016.

226. ** Windhab EJ, Dressler M, Feigl K, Fischer P, Megias-Alguacil D: **Emulsion processing—from single-drop deformation to design of complex processes and products**. *Chem Eng Sci* 2005, **60**:2101–2113.

227. Goddard J, Miller C: **An inverse for the jaumann derivative and some applications to the rheology of viscoelastic fluids**. *Rheol Acta* 1966, **5**:177–184.

228. Goddard JD, Miller C: **Nonlinear effects in the rheology of dilute suspensions**. *J Fluid Mech* 1967, **28**:657–673.

229. Oldroyd J: **Non-Newtonian effects in steady motion of some idealized elastico-viscous liquids**. *Proc Roy Soc Lond Math Phys Sci* 1958, **245**:278–297.

230. Oldroyd JG: **On the formulation of rheological equations of state**. *Proc Roy Soc Lond Math Phys Sci* 1950, **200**:523–541.

231. Pal R: **Shear viscosity behavior of emulsions of two immiscible liquids**. *J Colloid Interface Sci* 2000, **225**:359–366.

232. on Official Nomenclature AHC: **Symbols, Official symbols and nomenclature of the society of rheology**. *J Rheol* 2013, **57**: 1047–1055.